with Alexa Fluor 488 or Alexa Fluor 594 (Invitrogen) at room temperature for 1 h. All the antibodies are listed in Table S2.

Crystal Violet Staining

The human ESC-derived cells that had adhered to the wells were stained with 200 µl of 0.3% crystal violet solution at room temperature for 15 min. Excess crystal violet was then removed and the wells were washed three times. Fixed crystal violet was solubilized in 200 µl of 100% ethanol at room temperature for 15 min. Cell viability was estimated by measuring the absorbance at 595 nm of each well using a microtiter plate reader (Sunrise, Tecan).

LacZ Assay

The human ESC- and iPSC-derived cells were transduced with Ad-LacZ at 3,000 VP/cell for 1.5 h. After culturing for the indicated number of days, 5-bromo-4-chloro-3-indolyl β-D-galactopyranoside (X-Gal) staining was performed as described previously [15].

Supporting Information

Table S1 List of Taqman probes and primers used in this study.
(DOC)

Table S2 List of antibodies used in this study.
(DOC)

Figure S1 PrE cells formation from human ESCs on day 1 of differentiation. (A) The procedure for differentiation of human ESCs and iPSCs to ExEn cells by treatment with BMP4 (20 ng/ml) is presented schematically. (B) Human ESCs (H9) were morphologically changed during ExEn differentiation; when human ESCs were cultured with the medium containing BMP4 (20 ng/ml) for 5 days, the cells began to show flattened epithelial morphology. The scale bar represents 50 µm. (C–E) The tTemporal protein expression analysis during ExEn differentiation was performed by immunohistochemistry. The PrE markers COUP-TF1 [21] (red), SOX17 [14] (red), and SOX7 [14] (red) were detected on day 1. In contrast to the PS markers, the expression of the DE marker GSC [22] (red) was not detected and the level of the pluripotent marker NANOG (green) declined between day 0 and day 1. Nuclei were counterstained with DAPI (blue). The scale bar represents 50 µm.
(PDF)

Figure S2 Mesendoderm cells formation from human ESCs on day 3 of differentiation. (A) The procedure for differentiation of human ESCs and iPSCs to DE cells by treatment with Activin A (100 ng/ml) is presented schematically. hESF-GRO medium was supplemented with 5 factors and 0.5 mg/ml fatty acid free BSA, as described in the Materials and Methods. (B) Human ESCs (H9) were morphologically changed during DE differentiation; when human ESCs were cultured with the medium containing Activin A (100 ng/ml) for 5 days, the morphology of the cells began to show visible cell-cell boundaries. The scale bar represents 50 µm. (C–E) The tTemporal protein expression analysis during DE differentiation was performed by immunohistochemistry. The anterior PS markers FOXA2 [21] (red), GSC [22] (red), and SOX17 [14] (red) were adequately detected on day 3. The PS marker T [45] (red) was detected until day 3. In contrast to the PS markers, the expression of the pluripotent marker NANOG [24] (green) declined between day 2 and day 3. Nuclei were counterstained with DAPI (blue). The scale bar represents 50 µm.
(PDF)

Figure S3 Overexpression of SOX17 mRNA in human ESC (H9)-derived PS cells by Ad-SOX17 transduction. Human ESC-derived PS cells (day 1) were transduced with 3,000VP/cell of Ad-SOX17 for 1.5 h. On day 3 of differentiation, real-time RT-PCR analysis of the SOX17 expression was performed in Ad-LacZ-transduced cells and Ad-SOX17-transduced cells. On the y axis, the expression levels of undifferentiated human ESCs on day 0 was were taken defined as 1.0. All data are represented as the means±SD ($n = 3$).
(PDF)

Figure S4 Efficient transduction in Activin A-induced human ESC (H9)-derived cells by using a fiber-modified Ad vector containing the EF-1α promoter. Undifferentiated human ESCs and Activin A-induced human ESC-derived cells, which were cultured with the medium containing Activin A (100 ng/ml) for 0, 1, 2, 3, and 4 days, were transduced with 3,000 vector particles (VP)/cell of Ad-LacZ for 1.5 h. The day after transduction, X-gal staining was performed. The scale bar represents 100 µm. Similar results were obtained in two independent experiments.
(PDF)

Figure S5 Optimization of the time period for Ad-SOX17 transduction to promote DE differentiation from human iPSCs (Tic). Undifferentiated human iPSCs and Activin A-induced human iPSC-derived cells, which were cultured with the medium containing Activin A (100 ng/ml) for 0, 1, 2, 3, and 4 days, were transduced with 3,000 VP/cell of Ad-SOX17 for 1.5 h. Ad-SOX17-transduced cells were cultured with Activin A (100 ng/ml) until day 5, and then real-time RT-PCR analysis was performed. The horizontal axis represents the day on which the cells were transduced with Ad-SOX17. On the y axis, the expression levels of undifferentiated cells on day 0 was were taken defined as 1.0. All data are represented as the means±SD ($n = 3$).
(PDF)

Figure S6 Time course of LacZ expression in human ESC (H9)-derived mesendoderm cells transduced with Ad-LacZ. The hHuman ESC-derived mesendoderm cells (day 3) were transduced with 3,000 VP/cell of Ad-LacZ for 1.5 h. On days 4, 5, 6, 8, and 10, X-gal staining was performed. Note that human ESC-derived cells were passaged on day 5. The scale bar represents 100 µm. Similar results were obtained in two independent experiments.
(PDF)

Figure S7 Optimization of the time period for Ad-SOX17 transduction into Activin A-induced human ESC (H9)-derived cells. Undifferentiated human ESCs and Activin A-induced hESC-derived cells, which were cultured with the medium containing Activin A (100 ng/ml) for 0, 1, 2, 3, and 4 days, were transduced with 3,000 VP/cell of Ad-LacZ or Ad-SOX17 for 1.5 h. Ad-SOX17-transduced cells were cultured with Activin A (100 ng/ml) until day 5, then the cell viability was evaluated with crystal violet staining. The horizontal axis represents the day on which the cells were transduced with Ad-SOX17. On the y axis, the level of non-transduced cells was taken defined as 1.0. All data are represented as the means±SD (n = 3).
(PDF)

Figure S8 Model of differentiation of human ESCs and iPSCs into ExEn and DE cells by stage-specific SOX17 transduction. The ExEn and DE differentiation process is divided into at least two stages. In the first stage, human ESCs differentiate into either PrE cells by treatment with BMP4 (20 ng/ml) or mesendoderm cells by treatment with Activin A (100 ng/

ml). In the second stage, SOX17 promotes the further differentiation of each precursor cell into ExEn and DE cells, respectively. We have demonstrated that the efficient differentiation of these two distinct endoderm lineages is accomplished by stage-specific SOX17 transduction.
(PDF)

Acknowledgments

We thank Hiroko Matsumura and Misae Nishijima for their excellent technical support. We thank Mr. David Bennett and Ms. Ong Tyng Tyng for critical reading of the manuscript.

Author Contributions

Conceived and designed the experiments: K. Takayama MI K. Kawabata MFK HM. Performed the experiments: K. Takayama MI K. Tashiro. Analyzed the data: K. Takayama MI K. Kawabata K. Tashiro K. Katayama FS HM. Contributed reagents/materials/analysis tools: K. Kawabata K. Katayama FS TH MFK HM. Wrote the paper: K. Takayama K. Kawabata HM.

References

1. Enders AC, Given RL, Schlafke S (1978) Differentiation and migration of endoderm in the rat and mouse at implantation. Anat Rec 190: 65–77.
2. Gardner RL (1983) Origin and differentiation of extraembryonic tissues in the mouse. Int Rev Exp Pathol 24: 63–133.
3. Grapin-Botton A, Constam D (2007) Evolution of the mechanisms and molecular control of endoderm formation. Mech Dev 124: 253–278.
4. Tam PP, Kanai-Azuma M, Kanai Y (2003) Early endoderm development in vertebrates: lineage differentiation and morphogenetic function. Curr Opin Genet Dev 13: 393–400.
5. Thomson JA, Itskovitz-Eldor J, Shapiro SS, Waknitz MA, Swiergiel JJ, et al. (1998) Embryonic stem cell lines derived from human blastocysts. Science 282: 1145–1147.
6. Takahashi K, Tanabe K, Ohnuki M, Narita M, Ichisaka T, et al. (2007) Induction of pluripotent stem cells from adult human fibroblasts by defined factors. Cell 131: 861–872.
7. Yu J, Vodyanik MA, Smuga-Otto K, Antosiewicz-Bourget J, Frane JL, et al. (2007) Induced pluripotent stem cell lines derived from human somatic cells. Science 318: 1917–1920.
8. Xu RH, Chen X, Li DS, Li R, Addicks GC, et al. (2002) BMP4 initiates human embryonic stem cell differentiation to trophoblast. Nat Biotechnol 20: 1261–1264.
9. Pera MF, Andrade J, Houssami S, Reubinoff B, Trounson A, et al. (2004) Regulation of human embryonic stem cell differentiation by BMP-2 and its antagonist noggin. J Cell Sci 117: 1269–1280.
10. Seguin CA, Draper JS, Nagy A, Rossant J (2008) Establishment of endoderm progenitors by SOX transcription factor expression in human embryonic stem cells. Cell Stem Cell 3: 182–195.
11. Gouon-Evans V, Boussemart L, Gadue P, Nierhoff D, Koehler CI, et al. (2006) BMP-4 is required for hepatic specification of mouse embryonic stem cell-derived definitive endoderm. Nat Biotechnol 24: 1402–1411.
12. Niakan KK, Ji H, Maehr R, Vokes SA, Rodolfa KT, et al. (2010) Sox17 promotes differentiation in mouse embryonic stem cells by directly regulating extraembryonic gene expression and indirectly antagonizing self-renewal. Genes Dev 24: 312–326.
13. Inamura M, Kawabata K, Takayama K, Tashiro K, Sakurai F, et al. (2011) Efficient Generation of Hepatoblasts From Human ES Cells and iPS Cells by Transient Overexpression of Homeobox Gene HEX. Mol Ther 19: 400–407.
14. Kanai-Azuma M, Kanai Y, Gad JM, Tajima Y, Taya C, et al. (2002) Depletion of definitive gut endoderm in Sox17-null mutant mice. Development 129: 2367–2379.
15. Kawabata K, Sakurai F, Yamaguchi T, Hayakawa T, Mizuguchi H (2005) Efficient gene transfer into mouse embryonic stem cells with adenovirus vectors. Mol Ther 12: 547–554.
16. Koizumi N, Mizuguchi H, Utoguchi N, Watanabe Y, Hayakawa T (2003) Generation of fiber-modified adenovirus vectors containing heterologous peptides in both the HI loop and C terminus of the fiber knob. J Gene Med 5: 267–276.
17. Fujikura J, Yamato E, Yonemura S, Hosoda K, Masui S, et al. (2002) Differentiation of embryonic stem cells is induced by GATA factors. Genes Dev 16: 784–789.
18. Koutsourakis M, Langeveld A, Patient R, Beddington R, Grosveld F (1999) The transcription factor GATA6 is essential for early extraembryonic development. Development 126: 723–732.
19. Morrisey EE, Tang Z, Sigrist K, Lu MM, Jiang F, et al. (1998) GATA6 regulates HNF4 and is required for differentiation of visceral endoderm in the mouse embryo. Genes Dev 12: 3579–3590.
20. Kunath T, Strumpf D, Rossant J (2004) Early trophoblast determination and stem cell maintenance in the mouse--a review. Placenta 25 Suppl A: S32–38.
21. Sasaki H, Hogan BL (1993) Differential expression of multiple fork head related genes during gastrulation and axial pattern formation in the mouse embryo. Development 118: 47–59.
22. Blum M, Gaunt SJ, Cho KW, Steinbeisser H, Blumberg B, et al. (1992) Gastrulation in the mouse: the role of the homeobox gene goosecoid. Cell 69: 1097–1106.
23. Morrison GM, Oikonomopoulou I, Migueles RP, Soneji S, Livigni A, et al. (2008) Anterior definitive endoderm from ESCs reveals a role for FGF signaling. Cell Stem Cell 3: 402–415.
24. Mitsui K, Tokuzawa Y, Itoh H, Segawa K, Murakami M, et al. (2003) The homeoprotein Nanog is required for maintenance of pluripotency in mouse epiblast and ES cells. Cell 113: 631–642.
25. Shalaby F, Rossant J, Yamaguchi TP, Gertsenstein M, Wu XF, et al. (1995) Failure of blood-island formation and vasculogenesis in Flk-1-deficient mice. Nature 376: 62–66.
26. D'Amour KA, Agulnick AD, Eliazer S, Kelly OG, Kroon E, et al. (2005) Efficient differentiation of human embryonic stem cells to definitive endoderm. Nat Biotechnol 23: 1534–1541.
27. Shiojiri N (1984) The origin of intrahepatic bile duct cells in the mouse. J Embryol Exp Morphol 79: 25–39.
28. Ingelman-Sundberg M, Oscarson M, McLellan RA (1999) Polymorphic human cytochrome P450 enzymes: an opportunity for individualized drug treatment. Trends Pharmacol Sci 20: 342–349.
29. Murry CE, Keller G (2008) Differentiation of embryonic stem cells to clinically relevant populations: lessons from embryonic development. Cell 132: 661–680.
30. Qu XB, Pan J, Zhang C, Huang SY (2008) Sox17 facilitates the differentiation of mouse embryonic stem cells into primitive and definitive endoderm in vitro. Dev Growth Differ 50: 585–593.
31. Sherwood RI, Jitianu C, Cleaver O, Shaywitz DA, Lamenzo JO, et al. (2007) Prospective isolation and global gene expression analysis of definitive and visceral endoderm. Dev Biol 304: 541–555.
32. Shimoda M, Kanai-Azuma M, Hara K, Miyazaki S, Kanai Y, et al. (2007) Sox17 plays a substantial role in late-stage differentiation of the extraembryonic endoderm in vitro. J Cell Sci 120: 3859–3869.
33. Yasunaga M, Tada S, Torikai-Nishikawa S, Nakano Y, Okada M, et al. (2005) Induction and monitoring of definitive and visceral endoderm differentiation of mouse ES cells. Nat Biotechnol 23: 1542–1550.
34. Gadue P, Huber TL, Paddison PJ, Keller GM (2006) Wnt and TGF-beta signaling are required for the induction of an in vitro model of primitive streak formation using embryonic stem cells. Proc Natl Acad Sci U S A 103: 16806–16811.
35. Levinson-Dushnik M, Benvenisty N (1997) Involvement of hepatocyte nuclear factor 3 in endoderm differentiation of embryonic stem cells. Mol Cell Biol 17: 3817–3822.
36. Spence JR, Lange AW, Lin SC, Kaestner KH, Lowy AM, et al. (2009) Sox17 regulates organ lineage segregation of ventral foregut progenitor cells. Dev Cell 17: 62–74.
37. Mizuguchi H, Hayakawa T (2004) Targeted adenovirus vectors. Hum Gene Ther 15: 1034–1044.
38. Furue MK, Na J, Jackson JP, Okamoto T, Jones M, et al. (2008) Heparin promotes the growth of human embryonic stem cells in a defined serum-free medium. Proc Natl Acad Sci U S A 105: 13409–13414.
39. Makino H, Toyoda M, Matsumoto K, Saito H, Nishino K, et al. (2009) Mesenchymal to embryonic incomplete transition of human cells by chimeric OCT4/3 (POU5F1) with physiological co-activator EWS. Exp Cell Res 315: 2727–2740.
40. Nagata S, Toyoda M, Yamaguchi S, Hirano K, Makino H, et al. (2009) Efficient reprogramming of human and mouse primary extra-embryonic cells to pluripotent stem cells. Genes Cells 14: 1395–1404.
41. Mizuguchi H, Kay MA (1998) Efficient construction of a recombinant adenovirus vector by an improved in vitro ligation method. Hum Gene Ther 9: 2577–2583.
42. Mizuguchi H, Kay MA (1999) A simple method for constructing E1- and E1/E4-deleted recombinant adenoviral vectors. Hum Gene Ther 10: 2013–2017.
43. Tashiro K, Kawabata K, Sakurai H, Kurachi S, Sakurai F, et al. (2008) Efficient adenovirus vector-mediated PPAR gamma gene transfer into mouse embryoid bodies promotes adipocyte differentiation. J Gene Med 10: 498–507.
44. Maizel JV, Jr., White DO, Scharff MD (1968) The polypeptides of adenovirus. I. Evidence for multiple protein components in the virion and a comparison of types 2, 7A, and 12. Virology 36: 115–125.
45. Wilkinson DG, Bhatt S, Herrmann BG (1990) Expression pattern of the mouse T gene and its role in mesoderm formation. Nature 343: 657–659.

THE JOURNAL OF BIOLOGICAL CHEMISTRY VOL. 286, NO. 25, pp. 22403–22413, June 24, 2011

Dendritic Cell-specific Intercellular Adhesion Molecule 3-grabbing Non-integrin (DC-SIGN) Recognizes a Novel Ligand, Mac-2-binding Protein, Characteristically Expressed on Human Colorectal Carcinomas*

Received for publication, December 22, 2010, and in revised form, March 24, 2011 Published, JBC Papers in Press, April 22, 2011, DOI 10.1074/jbc.M110.215301

Motohiro Nonaka[‡1], Bruce Yong Ma[‡§¶2], Hirotsugu Imaeda[‖], Keiko Kawabe[‡], Nobuko Kawasaki[‡], Keiko Hodohara[‖], Nana Kawasaki[**], Akira Andoh[‡‡], Yoshihide Fujiyama[‖], and Toshisuke Kawasaki[‡3]

From the [‡]Research Center for Glycobiotechnology, Ritsumeikan University, Shiga 525-0058, [‖]Department of Medicine, and [‡‡]Division of Mucosal Immunology, Graduate School of Medicine, Shiga University of Medical Science, Shiga 520-2192, [**]Division of Biological Chemistry and Biologicals, National Institute of Health Sciences, Tokyo 158-8501, [§]Department of Computer Science and Systems Engineering, Muroran Institute of Technology, Hokkaido 050-8585, Japan, and [¶]School of Pharmaceutical Engineering and Life Science, Changzhou University, Jiangsu 213164, China

Dendritic cell (DC)-specific intercellular adhesion molecule-3-grabbing non-integrin (DC-SIGN) is a type II transmembrane C-type lectin expressed on DCs such as myeloid DCs and monocyte-derived DCs (MoDCs). Recently, we have reported that DC-SIGN interacts with carcinoembryonic antigen (CEA) expressed on colorectal carcinoma cells. CEA is one of the most widely used tumor markers for gastrointestinal cancers such as colorectal cancer. On the other hand, other groups have reported that the level of Mac-2-binding protein (Mac-2BP) increases in patients with pancreatic, breast, and lung cancers, virus infections such as human immunodeficiency virus and hepatitis C virus, and autoimmune diseases. Here, we first identified Mac-2BP expressed on several colorectal carcinoma cell lines as a novel DC-SIGN ligand through affinity chromatography and mass spectrometry. Interestingly, we found that DC-SIGN selectively recognizes Mac-2BP derived from some colorectal carcinomas but not from the other ones. Furthermore, we found that the α1-3,4-fucose moieties of Le glycans expressed on DC-SIGN-binding Mac-2BP were important for recognition. DC-SIGN-dependent cellular interactions between immature MoDCs and colorectal carcinoma cells significantly inhibited MoDC functional maturation, suggesting that Mac-2BP may provide a tolerogenic microenvironment for colorectal carcinoma cells through DC-SIGN-dependent recognition. Importantly, Mac-2BP was detected as a predominant DC-SIGN ligand expressed on some primary colorectal cancer tissues from certain parts of patients in comparison with CEA from other parts, suggesting that DC-SIGN-binding Mac-2BP bearing tumor-associated Le glycans may become a novel potential colorectal cancer biomarker for some patients instead of CEA.

Dendritic cells (DCs)[4] play a critical role in initiating adaptive immunity by uptaking foreign antigens at the periphery, undergoing maturation during migration to lymph nodes and presenting antigen-derived peptides to naïve T cells (1, 2). For effective recognition of antigens, DCs exploit a wide range of pattern recognition receptors such as Toll-like receptors and C-type lectins (3–5). DC-specific intercellular adhesion molecule-3-grabbing non-integrin (DC-SIGN; CD209) is a type II transmembrane C-type lectin expressed on myeloid DCs in the dermis, mucosae, lymph nodes, and monocyte-derived DCs (MoDCs) (6, 7). DC-SIGN binds to "self" glycan ligands found on human cells and to "foreign" glycans of bacterial or parasitic pathogens, and specifically recognizes glycoconjugates containing mannose (Man), fucose (Fuc), and nonsialylated Lewis $(Le)^a/Le^b$ epitope structures in a Ca^{2+}-dependent manner (8). Through recognition of these glycans, DC-SIGN functions as an adhesion receptor and mediates the binding and internalization of foreign pathogens such as viruses (human immunodeficiency virus and hepatitis C virus), yeasts, bacteria (*Mycobacterium tuberculosis*), and parasites (3).

Recently, we and another group (9, 10) found that DC-SIGN recognizes colorectal carcinoma cells through carcinoembryonic antigen (CEA). DC-SIGN-binding CEA contained tumor-associated Le glycans, which were important for cellular interactions between DCs and colorectal carcinoma cells *in situ*. It is evident that the expression of CEA is limited and can be

* This work was supported by Grants-in-aid for Scientific Research B 20370052 (to T. K.) and C 21590543 (to B. Y. M.), for Young Scientists Start-up 20890255 (to M. N.), and for Japan Society for the Promotion of Science (JSPS) Fellows 22-9530 (to M. N.) from JSPS, the Ministry of Education, Culture, Sports, Science, and Technology of Japan, JSPS Core-to-Core Program Strategic Research Networks (17005) from JSPS, and Research Proposal Grants from Japan Foundation for Applied Enzymology (Osaka, Japan; to B. Y. M.).

[1] A JSPS Research Fellow.

[2] To whom correspondence may be addressed: Research Center for Glycobiotechnology, Ritsumeikan University, Noji-Higashi, Kusatsu, Shiga 525-0058, Japan. Tel.: 81-77-561-3444; Fax: 81-77-561-3496; E-mail: bruceyongma@gmail.com.

[3] To whom correspondence may be addressed: Research Center for Glycobiotechnology, Ritsumeikan University, Noji-Higashi, Kusatsu, Shiga 525-0058, Japan. Tel.: 81-77-561-3444; Fax: 81-77-561-3496; E-mail: tkawasak@fc.ritsumei.ac.jp.

[4] The abbreviations used are: DC, dendritic cell; DC-SIGN, DC-specific intercellular adhesion molecule-3-grabbing non-integrin; rhDC-SIGN-Fc, recombinant human DC-SIGN-human IgG-Fc fusion protein; pAb, polyclonal Ab; Mac-2BP, Mac-2-binding protein; CEA, carcinoembryonic antigen; MoDC, monocyte-derived DC; Le, Lewis; PHA, phytohaemagglutinin; AAL, *Aleuria aurantia* agglutinin; PNGase, peptide *N*-glycosidase; M-CSF, macrophage colony-stimulating factor.

detected only in cancer and embryonic tissues. This glycoprotein is one of the most widely used tumor markers for gastrointestinal cancers such as colorectal carcinomas. However, its sensitivity and specificity are not high, particularly for early stages of the disease such as Dukes A or B stages. Based on our studies, we hypothesized that DC-SIGN may also be involved in the recognition of other glycoproteins, as novel potential biomarkers, expressed on colorectal cancers.

In this study, we first identified Mac-2-binding protein (Mac-2BP) expressed on colorectal carcinoma cells as a novel DC-SIGN ligand through affinity chromatography and mass spectrometry. Mac-2BP, also known as 90K or galectin-3BP, is a secretory glycoprotein expressed on various normal epithelial cells and in human bodily fluids. It has been reported that the level of Mac-2BP increases in patients with pancreatic, breast, and lung cancer, virus infections such as acquired immunodeficiency syndrome and hepatitis C, and autoimmune diseases (11). However, most of the immunological significance of Mac-2BP on colorectal carcinomas remains unknown.

In addition, we found that DC-SIGN-dependent cellular interactions between immature MoDCs and colorectal carcinoma cells mainly expressing Mac-2BP were able to significantly inhibit LPS-induced MoDC functional maturation. Furthermore, we also detected Mac-2BP as a predominant DC-SIGN ligand expressed on some primary colorectal cancer tissues from certain parts of patients in comparison with CEA from the other parts. Therefore, we suggest that Mac-2BP carrying fucosylated glycans may become a novel potential colorectal cancer biomarker for some CEA-low or -negative colorectal cancer patients, and the novel function of DC-SIGN may, at least in part, underlie for its potential use as a novel diagnostic sensor for some colorectal cancer patients through recognition of CEA and Mac-2BP.

EXPERIMENTAL PROCEDURES

Reagents and Antibodies—Recombinant human DC-SIGN-human IgG-Fc fusion protein (rhDC-SIGN-Fc), anti-human DC-SIGN mAb, and anti-Mac-2BP polyclonal antibody (pAb) were purchased from R&D Systems (Minneapolis, MN). Anti-Mac-2BP mAb was from Bender Medsystems (Burlingame, CA). Anti-Le^a, Le^b, and CEA mAbs were from Abcam (Cambridge, MA). Anti-human CD83 and CD86 mAbs were from BD Biosciences. Alexa Fluor 488- or 546-conjugated secondary antibodies were from Invitrogen. HRP-conjugated anti-FLAG antibody and Ultrapure lipopolysaccharide from *Escherichia coli* 0111:B4 were from Sigma-Aldrich. Anti-human DC-SIGN pAb (C-20) was from Santa Cruz Biotechnology (Santa Cruz, CA). All chemicals for gel electrophoresis and Western blotting were purchased from Nacalai Tesque, ATTO Corp. (Tokyo, Japan), Bio-Rad, Thermo Fisher Scientific (Waltham, MA), or Invitrogen.

Cell Lines, Cell Culture, and Immature MoDCs and Maturation of Immature MoDCs—Human colon tumor cell lines COLO205 and SW1116 and human hepatoma cell line HLF were cultured as described previously (10). All of the cell lines were obtained from ATCC. DC-SIGN-expressing HLF cells (HLF-DC-SIGN) were generated by transfection of the pcDNA3-DC-SIGN plasmid (10) with Lipofectamine 2000 reagent (Invitrogen), and then selection was performed in complete medium containing 1 mg/ml G418 (Invitrogen) for stable transfectants. Isolation of human peripheral blood mononuclear cells from healthy donors, positive selection of $CD14^+$ cells, induction of immature MoDCs, and maturation of MoDCs were conducted as described previously (10) in accordance with the Declaration of Helsinki. DC maturation was confirmed by expression of CD83, a DC-specific maturation marker, and CD86, a costimulatory molecule, on mature but not immature DCs.

Cellular Adhesion Assay—HLF-DC-SIGN or HLF cells were incubated into confluent culture at 37 °C in 96-well plates and then COLO205 cells, which had been prelabeled with the green fluorescent dye calcein-AM (Invitrogen), were added onto the wells and incubated for 1 h. After unbound cells were removed with wash buffer (0.5% BSA, 150 mM NaCl, 20 mM Tris/HCl (pH 7.5), and 1 mM $CaCl_2$), cells on the plates were lysed with lysis buffer (20 mM Tris/HCl (pH 7.5), and 0.1% SDS) and analyzed by fluorometry at 488 nm. Population of adhered COLO205 cells was calculated as the percentage of maximal binding, which was determined by the lysed total amount of added calcein-AM-labeled cells (100% adhesions).

ELISA Analysis—For analysis of DC-SIGN binding to proteins secreted by HLF, COLO205, or SW1116 cells, culture supernatants were mixed with coating buffer (Na_2CO_3 buffer, pH 9.6) and then coated onto NUNC maxisorp 96-well plates (Nalge Nunc) overnight at 4 °C. Mannan was used as a positive control. Then, the plates were blocked with 3% BSA in coating buffer for 1 h at room temperature, washed with TBS (pH 7.6) containing 0.05% Tween 20, and then incubated with 0.4 μg/ml rhDC-SIGN-FLAG in 1% BSA in TBS (pH 7.6) containing 5 mM $CaCl_2$ for 1 h at room temperature. After the plates had been washed, HRP-conjugated anti-FLAG mAb was added, followed by incubation for 1 h.

For analysis of DC-SIGN binding to Mac-2BP secreted by human hepatoma and colorectal carcinoma cell lines, 1 μg/ml anti-Mac-2BP pAbs were precoated onto 96-well plates overnight at 4 °C. After blocking, culture supernatants of HepG2, HLF, COLO205, LS180, or SW1116 cells were added, followed by incubation for 1 h at room temperature. DC-SIGN binding was assayed using rhDC-SIGN-FLAG, as described above.

For quantitative kinetic data of association between DC-SIGN and Mac-2BP, 5 ng/well of Mac-2BP captured onto plates were reacted for 2 h with different concentrations (0.063–8.000 nM) of rhDC-SIGN-FLAG in the presence of 5 mM $CaCl_2$. Quantitative kinetic data (K_d app and B_{max}) were calculated based on the amounts of total and unbound rhDC-SIGN-FLAG using a nonlinear regression model by GraphPad Prism software (version 4.0c). DC-SIGN was regarded as a tetramer.

For determination of the glycan profile of COLO205-derived Mac-2BP, anti-Mac-2BP pAb was precoated onto 96-well plates overnight at 4 °C. After blocking, culture supernatants of HLF or COLO205 cells were added, followed by incubation for 1 h at room temperature. Then the captured Mac-2BP was incubated with biotin-conjugated plant lectins (phytohemeagglutinin (PHA)-L4, *Lycopersicon esculentum* agglutinin, and *Aleuria aurantia* agglutinin (AAL)), followed by incuba-

tion with HRP-conjugated avidin. After development, binding was quantitated by measuring the absorbance at 450 nm using a Multilabel Counter (PerkinElmer Life Sciences) in accordance with the manufacturer's instructions. All experiments were performed in triplicate and were repeated a minimum of three times.

Preparation of Membrane Fractions, Affinity Chromatography, and Mass Spectrometry—Affinity sepharoses were prepared using Seize X Protein G Immunoprecipitation kit (Thermo Fisher Scientific). According to the manufacturer's instructions, rhDC-SIGN-Fc and hIgG-Fc proteins were immobilized to Protein G-Sepharose using the cross-linker disuccinimidyl suberate. Cells were homogenized in homogenization buffer (10 mM Tris/HCl (pH 7.6), 0.5 mM $MgCl_2$, and protease inhibitor mixture), and then tonicity was restored into 150 mM NaCl. The homogenate was centrifuged at 500 × *g* for 5 min at 4 °C to remove cell debris and nuclei. The supernatant was supplemented with EDTA to 5 mM and then centrifuged at 150,000 × *g* for 45 min at 4 °C. The resulting total membrane pellet was solubilized with lysis buffer (150 mM NaCl, 20 mM Tris/HCl (pH 7.5), 1 mM EDTA, 1% Triton X-100, and protease inhibitor mixture) for 60 min at 4 °C and then centrifuged at 10,000 × *g* for 60 min at 4 °C. The supernatant was saved as the solubilized COLO205 membrane proteins and was applied to a rhDC-SIGN-Fc or hIgG-Fc affinity column. After the column had been washed with TBS buffer (pH 7.5) containing 5 mM $CaCl_2$ and 0.1% Triton X-100, the proteins bound to the column were eluted with TBS buffer (pH 7.5) containing 10 mM EDTA and 0.1% Triton X-100. The EDTA-eluted fractions were buffer-exchanged, applied again to the same column and then eluted with TBS buffer (pH 7.5) containing 50 mM Man. The secondly eluted proteins were resolved on a 5–20% Tris/HCl gradient gel (ATTO Corporation) and then stained with a silver staining kit (Wako Pure Chemical Industries). Bands were excised from the gel and subjected to in-gel digestion. The peptides released from the gel were subjected to LC/MS/MS with a linear ion trap mass spectrometer (LTQ, Thermo Fisher Scientific) interfaced on-line with a nano HPLC (Paradigm, Michrom BioResources, Auburn, CA). The eluents consisted of H_2O containing 2% CH_3CN and 0.1% formic acid (Pump A), and 90% CH_3CN and 0.1% formic acid (Pump B), and the peptides were eluted with a linear gradient of 5–80% from Pump B. Data-dependent MS/MS acquisition was performed for the most intense ions as precursors. Proteins were identified by searching the Swiss-Prot *Homo sapiens* and NCBInr database (human) using the Mascot search engine (Matrixscience, London, UK) and Bioworks search engine (Thermo Fisher Scientific), respectively.

Ligand Precipitation, Immunoprecipitation, and Immunoblotting—Solubilized membrane proteins from HLF, COLO205, and SW1116 cells were prepared as described above, and used as ligand precipitation, immunoprecipitation, and immunoblot samples. To identify the proteins carrying DC-SIGN carbohydrate ligands on colorectal carcinomas, precipitation was performed using rhDC-SIGN-Fc- or rhIgG-Fc-Protein G beads, and the bound proteins were eluted with EDTA as immunoblot samples. The samples were resolved on 5–20% gradient SDS-PAGE gels (ATTO Corp.) and then transferred to nitrocellulose membranes, followed by immunoblot detection with specific antibodies. For visualization, a Super-Signal West Pico Chemiluminescent kit (Thermo Fisher Scientific) was used with HRP-conjugated anti-mouse or anti-goat IgG. The amounts of SDS-PAGE loading proteins from HLF, COLO205, and SW1116 cells were adjusted on the basis of cell numbers, and we confirmed by Bradford method that whole membrane lysates contained 15–20 μg/lane and culture supernatant contained 27–32 μg/lane of comparable proteins (data not shown).

Glycan Digestion Assay—For peptide-*N*-glycosidase (PNGase) F treatment, membrane proteins prepared from COLO205 cells, as described above, were adjusted to 10 mM EDTA, 0.1% SDS, and 0.1% Nonidet P-40 and then incubated overnight with or without PNGase F at 37 °C. After replacement in Hepes buffer (pH 7.5)-0.15 M NaCl by ultrafiltration, DC-SIGN ligands were precipitated with rhDC-SIGN-Fc, followed by SDS-PAGE and immunoblotting with anti-Mac-2BP pAb. For α1-3,4-fucosidase treatment, a membrane pellet of COLO205 cells prepared as described above was suspended in 20 mM KH_2PO_4 (pH 5.0) buffer containing 1% Nonidet P-40, followed by incubation overnight with or without α1-3,4-fucosidase at 37 °C, and then ligand precipitation with rhDC-SIGN-Fc, anti-Le^a or -Le^b mAb, SDS-PAGE, and immunoblotting with anti-Mac-2BP pAb.

MoDC Functional Maturation—To determine the effect of a MoDC-COLO205-cocultured supernatant on LPS-induced functional maturation of MoDCs, immature MoDCs were incubated in a MoDC-cultured or MoDC-SW1116-cocultured supernatant for 3 days in the presence of IL-4 (500 units/ml), GM-CSF (800 units/ml), and LPS (1 ng/ml). Supernatant of MoDC, which cultured in the presence of anti-DC-SIGN pAb, was used as a control. Cultures were replenished with fresh supernatant on the second day. The effect on MoDC functional maturation was determined by cell-surface expression of CD83, a DC-specific maturation marker, and CD86, a costimulatory molecule on mature DCs, using FACS Calibur™, and the mean fluorescent intensity was calculated with CELLQUEST software™ (BD Biosciences). All experiments were performed in triplicate and were repeated a minimum of three times.

Histochemistry—Clinical colorectal cancer tissue specimens were purchased from SuperBioChips Laboratories (Seoul, Korea), or obtained from Shiga University of Medical Science with informed consent. This project was approved by the ethics committee of Shiga University of Medical Science. Following deparaffinization and hydration of paraffin-embedded tissue sections, antigen retrieval was performed by steaming in citrate buffer (pH 6.0). After blocking with 1% BSA, the slides were incubated with 1 μg/ml of anti-Mac-2BP pAb followed by Alexa Fluor 546-conjugated secondary Ab (for anti-Mac-2BP staining), anti-CEA mAb (1:50) followed by Alexa Fluor 488-conjugated secondary Ab (for anti-CEA staining), and/or 1 μg/ml of allophycocyanin-conjugated rhDC-SIGN-FLAG (for direct rhDC-SIGN staining, donor 1) or rhDC-SIGN-FLAG followed by anti-FLAG mAb and Alexa Fluor 488-conjugated secondary Ab (for indirect rhDC-SIGN staining, donor 2), and then washed and mounted. To observe the expression of DC-SIGN ligands on COLO205 cells, cells were stained with 1

μg/ml of rhDC-SIGN-allophycocyanin and anti-Mac-2BP pAb, followed by Alexa Fluor 488-conjugated secondary Ab in the presence of $CaCl_2$ or EDTA. To investigate cellular interactions between immature MoDCs and COLO205 cells, cells were coincubated for 1 h at 37 °C and then stained with 1 μg/ml of anti-DC-SIGN mAb and anti-Mac-2BP pAb or anti-Le^b mAb, followed by Alexa Fluor 488- and 546-conjugated secondary Abs. The cellular interactions were visualized by laser confocal microscopy.

Statistical Analysis—The results are expressed as the means ± S.D. of data obtained in three experiments performed in triplicate. Statistical significance was determined by means of Student's *t* test.

RESULTS

DC-SIGN-mediated Cellular Adhesions and Mac-2BP Identified as a Novel DC-SIGN Ligand on Colorectal Carcinoma Cells—To determine whether or not DC-SIGN-expressing cells interact with human colorectal carcinoma cells, we coincubated either human hepatoma HLF cells or DC-SIGN-expressing HLF (HLF-DC-SIGN) cells with COLO205 cells. As shown in Fig. 1*A*, COLO205 cells significantly bound to HLF-DC-SIGN cells compared with control HLF cells, indicating that DC-SIGN is sufficiently involved in the cellular adhesions through interaction with DC-SIGN ligands expressed on COLO205 cells.

To completely isolate DC-SIGN ligands expressed on COLO205, the ligand glycoproteins from solubilized membrane fractions were purified by an affinity column of recombinant human DC-SIGN-Fc (rhDC-SIGN-Fc) and then analyzed by nano-LC/MS/MS, as described under "Experimental Procedures." The two major silver-stained bands, which were independent of the Fc portion of the DC-SIGN-Fc chimeric protein, indicated by the arrows (Fig. 1*B*) from rhDC-SIGN-Fc column were identified as matured and degraded Mac-2BP, respectively (Fig. 1*C*).

On the other hand, we previously identified CEA as the main DC-SIGN ligand expressed on SW1116 cells, another human colorectal carcinoma cell line. Therefore, we compared the expression levels of Mac-2BP and CEA between COLO205 and SW1116 cells by confocal microscopy. As shown in Fig. 1*D*, the cell-surface expression of Mac-2BP was markedly higher on COLO205 than SW1116 cells. In contrast, CEA could hardly be detected on COLO205 cells compared with its abundant expression on SW1116 cells.

Next, to confirm the interaction of DC-SIGN with Mac-2BP *in vitro*, DC-SIGN ligands purified from COLO205, SW1116, and human hepatoma HLF cells were immunoblotted with anti-Mac-2BP pAb (Fig. 1*E*) or anti-CEA mAb (Fig. 1*F*). The results showed that COLO205-derived Mac-2BP, but not HLF or SW1116-derived Mac-2BP, apparently interacted with rhDC-SIGN (Fig. 1*E*). In contrast, we observed high-level expression of CEA on SW1116 cells and its distinct association with rhDC-SIGN (Fig. 1*F*), whereas we could not detect any association of COLO205-derived CEA with rhDC-SIGN. Confocal microscopy also showed that Mac-2BP (*green*) was substantially colocalized with allophycocyanin-fluoresceinated rhDC-SIGN (*red*) on COLO205 cells in a Ca^{2+}-dependent manner (Fig. 1*G*). These findings indicated that Mac-2BP is a novel DC-SIGN ligand expressed on colorectal carcinoma cells and that DC-SIGN selectively interacts with Mac-2BP expressed on particular carcinoma cells as opposed to CEA.

DC-SIGN Binds to Mac-2BP Secreted by Several Colorectal Carcinoma Cell Lines—Mac-2BP and CEA were known originally as secretory proteins. Therefore, we examined whether or not DC-SIGN ligands existed in COLO205-, SW1116-, or HLF-cultured supernatants. As shown in Fig. 2*A*, ELISA analysis revealed that DC-SIGN ligand glycoproteins could be detected in a Ca^{2+}-dependent manner in both COLO205- and SW1116-cultured supernatants, but not in a HLF-cultured supernatant.

Next, to verify that DC-SIGN interacts with secreted CEA and Mac-2BP, purified DC-SIGN ligands from HLF-, COLO205-, and SW1116-cultured supernatants were immunoblotted with anti-Mac-2BP pAb and anti-CEA mAb, respectively. Interestingly, only Mac-2BP secreted by COLO205 cells, but not by HLF or SW1116 cells, interacted with rhDC-SIGN (Fig. 2*B*). On the other hand, CEA, which can interact with DC-SIGN, was only observed in the SW1116-cultured supernatant (Fig. 2*C*). Moreover, we investigated the interaction of DC-SIGN with Mac-2BP secreted by several other human hepatoma and colorectal carcinoma cell lines (Fig. 2*D*). The ELISA data showed that the human hepatoma HepG2 and HLF, and human colorectal carcinoma COLO205, LS180, and SW1116 cell lines all apparently expressed Mac-2BP (Fig. 2*D*, *upper panel*); however, only the COLO205- and LS180-derived Mac-2BP had the ability to interact with rhDC-SIGN (*lower panel*), indicating that parts of colorectal carcinomas can secrete DC-SIGN-recognizing Mac-2BP. These results also suggest that distinct glycoforms of Mac-2BP exist in different colorectal carcinomas.

DC-SIGN Binds to Mac-2BP from Colorectal Carcinoma Cells in Ca^{2+}-dependent and Dose-dependent Manners—To quantitatively characterize the direct association between DC-SIGN and COLO205-derived Mac-2BP, we performed ELISA experiments. As shown in Fig. 3*A*, the interactions were monitored as the changes in the ELISA responses, and the Ca^{2+} chelator EDTA completely blocked the interactions, suggesting that DC-SIGN directly binds to glycans on Mac-2BP in a dose-dependent manner, and the interaction occurs in a Ca^{2+}-dependent manner and the CRD of DC-SIGN mediates the binding.

Moreover, their affinity level was shown to be extremely high when the apparent dissociation constant (K_d app = 2.50 (±0.66)) was calculated by fitting a curve using nonlinear regression model (Fig. 3*B*). These results suggest the potential physiological interaction between DC-SIGN and Mac-2BP in the colon microenvironment.

DC-SIGN Recognizes Fucose Residues of Le N-Glycans on Mac-2BP from Colorectal Carcinoma Cells—To determine whether or not interaction of Mac-2BP with DC-SIGN is *N*-glycan-dependent, Mac-2BP purified from COLO205 cells was treated with PNGase F and then precipitated with rhDC-SIGN. Fig. 4*A* shows that the Mac-2BP band shifted from 90 to 65 kDa on PNGase F treatment and that the PNGase F-treated form had completely lost the ability to bind rhDC-SIGN, indicating

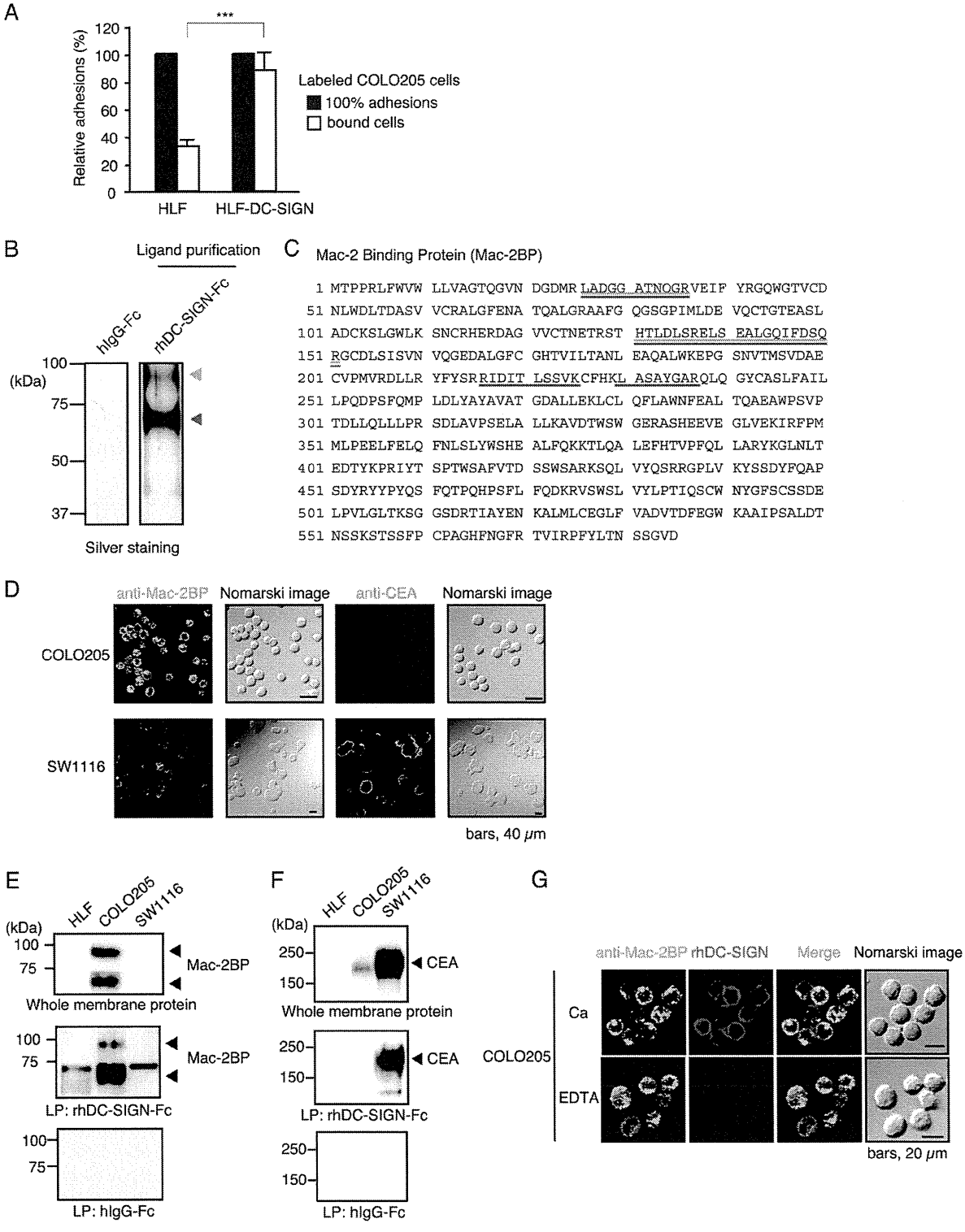

FIGURE 1. **Identification of Mac-2BP expressed on colorectal carcinomas as a novel ligand for DC-SIGN.** *A*, DC-SIGN-mediated cellular adhesions with COLO205 cells. HLF or HLF-DC-SIGN cells bound with calcein-AM-labeled COLO205 cells were lysed and analyzed by fluorometry at 488 nm. The relative adhesions are shown. *Error bars* indicate S.D. ($n = 3$). *B*, purification of DC-SIGN ligands expressed on COLO205 cells. DC-SIGN ligands were purified with a DC-SIGN affinity column and then detected by silver staining. The *arrowheads* indicate the elution positions of the purified DC-SIGN ligands. The molecular mass markers are shown on the *left*. *C*, identification of DC-SIGN novel ligands by MS. The purified DC-SIGN ligand bands were analyzed by MS. The identified peptides are shown in *green* (*upper band*) or *red* (*lower band*), respectively. *D*, confocal microscopic images of the expressions of Mac-2BP and CEA on COLO205 and SW1116 cells. Cells were stained with anti-Mac-2BP pAb or anti-CEA mAb (*green*). Nomarski images are shown on the *right*. *E* and *F*, ligand precipitation (*LP*) analysis of the interaction of DC-SIGN with CEA or Mac-2BP. Solubilized membrane proteins of HLF, COLO205, and SW1116 cells were precipitated with rhDC-SIGN-Fc or hIgG-Fc, and then EDTA-eluted DC-SIGN ligands were detected by immunoblotting using anti-Mac-2BP pAb (*E*) or anti-CEA mAb (*F*). *G*, confocal microscopic images of the interactions between DC-SIGN and Mac-2BP on COLO205 cells. The cells were costained with anti-Mac-2BP pAb (*green*) and rhDC-SIGN-allophycocyanin (*red*) in the presence of $CaCl_2$ or EDTA.

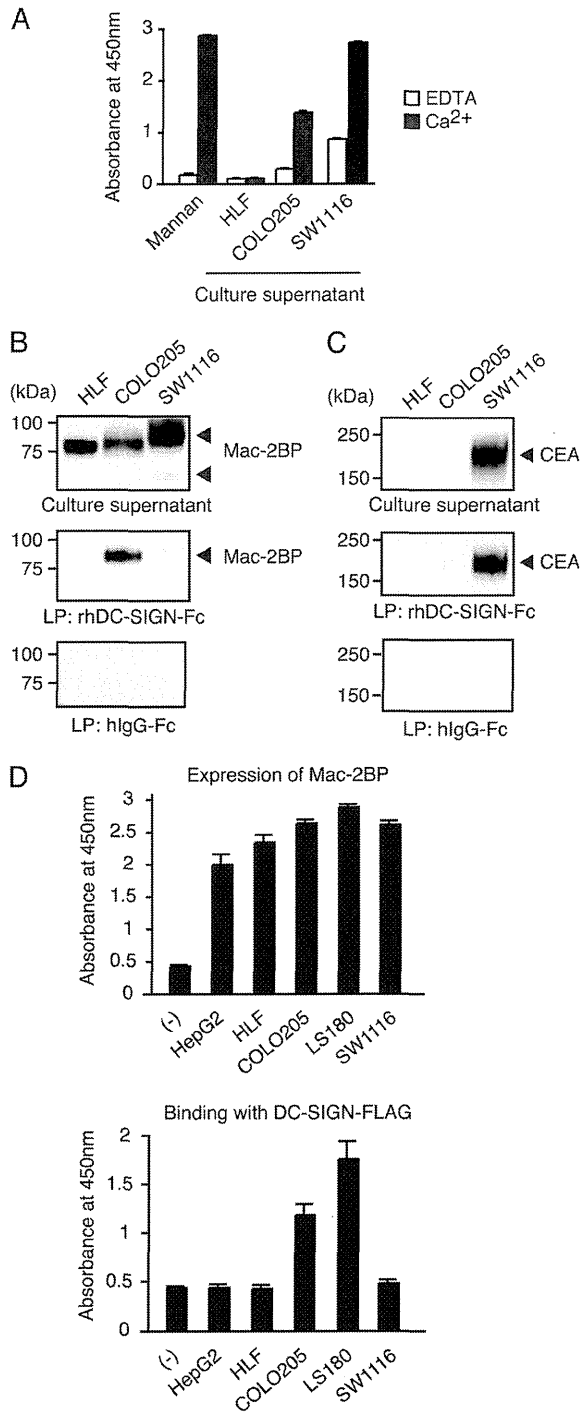

FIGURE 2. **Culture supernatants derived from colorectal carcinoma cells contain secreted Mac-2BP that can be recognized by DC-SIGN.** *A*, culture supernatant of colorectal carcinoma cells contain DC-SIGN-ligands. Total culture supernatant proteins from HLF, COLO205, and SW1116 cells, coated onto plates, were detected with rhDC-SIGN in the presence of 5 mM $CaCl_2$ or EDTA. Mannan was used as a positive control for DC-SIGN binding. *Error bars* indicate S.D. ($n = 3$). *B* and *C*, DC-SIGN interacts selectively with COLO205-derived Mac-2BP or SW1116-derived CEA contained in culture supernatants. A total culture supernatant and purified DC-SIGN ligands from HLF, COLO205, or SW1116 cells were immunoblotted with anti-Mac-2BP pAb or anti-CEA mAb. *D*, colorectal carcinoma cells secrete Mac-2BP that can be recognized by DC-SIGN. Mac-2BPs from human hepatoma HepG2 and HLF and colorectal carcinoma COLO205, LS180, and SW1116 cells were captured with anti-Mac-2BP pAb and then detected with anti-Mac-2BP mAb (*upper panel*) or with rhDC-SIGN-FLAG (*lower panel*), respectively. *Error bars* indicate S.D. ($n = 3$).

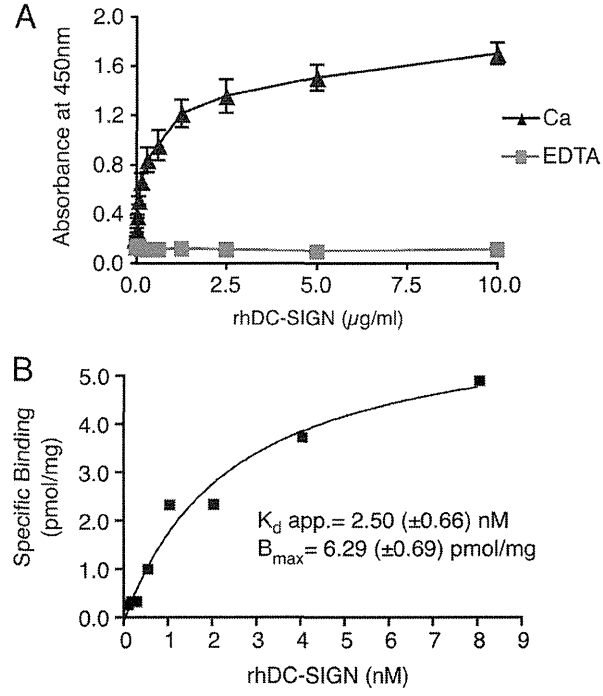

FIGURE 3. **Biochemical analysis of the interaction between DC-SIGN and Mac-2BP.** *A*, DC-SIGN-dependent interaction with COLO205-derived Mac-2BP. Mac-2BP, captured with anti-Mac-2BP pAb onto plates, was detected with different concentrations of rhDC-SIGN-FLAG in the presence of 5 mM $CaCl_2$ or EDTA. *Error bars* indicate S.D. ($n = 3$). *B*, quantitative kinetic analysis for association between DC-SIGN and Mac-2BP. The apparent (*app.*) dissociation constant (K_d app.) and B_{max} were calculated based on the amounts of total and unbound rhDC-SIGN-FLAG using a nonlinear regression model.

that the *N*-glycans on Mac-2BP mediate the interaction with DC-SIGN.

We next examined whether or not DC-SIGN-binding Mac-2BP expresses characteristic glycans by ELISA involving commonly used plant lectins (Fig. 4*B*). Well-coated Mac-2BP was incubated with three plant lectins, PHA-L4, *Lycopersicon esculentum* agglutinin, and AAL, respectively. *Lycopersicon esculentum* agglutinin, which predominantly recognizes polylactosamine glycans, exhibited a high degree of binding to HLF-derived Mac-2BP and a low degree of binding to COLO205-derived Mac-2BP. Whereas PHA-L4, which recognizes β1-6 branched GlcNAc glycans, exhibited almost the same degree of binding to HLF- and COLO205-derived Mac-2BPs, suggesting that β1-6 branched GlcNAc glycans are not the direct moieties for DC-SIGN binding. Interestingly, fucose-binding AAL lectin exhibited much stronger affinity with COLO205-derived than HLF-derived Mac-2BP.

AAL lectin exhibits a high affinity for α-fucosyl residues in the cores of *N*-linked glycans and Le glycans such as Le^a, Le^b, Le^x, Le^y, sialyl-Le^x, and sialyl-Le^x. Because DC-SIGN exhibits the highest affinity to Le glycans, but not to sialylated Le glycans, we hypothesized that fucose residues on Le glycans may directly mediate the interaction between DC-SIGN and COLO205-derived Mac-2BP. To prove this, we treated Mac-2BP with α1-3,4-fucosidase, an enzyme that specifically cleaves α1-3,4-bound fucose of Le^a, Le^b, Le^x, and Le^y. As shown in Fig. 4*C*, the defucosylated Mac-2BP had almost completely lost the ability to interact with DC-SIGN. Confocal microscopy also

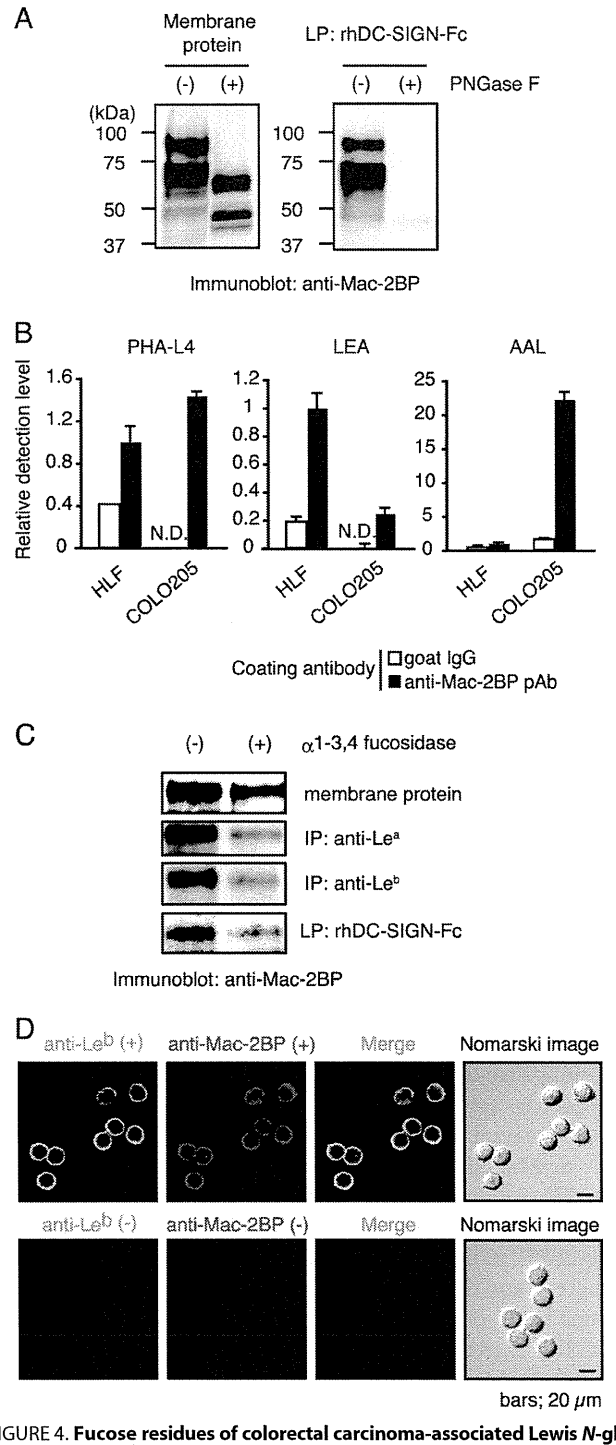

FIGURE 4. **Fucose residues of colorectal carcinoma-associated Lewis *N*-glycans expressed on COLO205-derived Mac-2BP are essential for DC-SIGN binding.** *A*, *N*-glycans of COLO205-derived Mac-2BP are essential for DC-SIGN binding. COLO205 membrane proteins were incubated with or without PNGase F, and then total membrane proteins (*left*) and subsequently purified DC-SIGN-ligands (*right*) were immunoblotted with anti-Mac-2BP pAb. *B*, determination for the Mac-2BP glycan profile by ELISA. COLO205-derived Mac-2BP glycoproteins captured with pre-coated anti-Mac-2BP pAb were detected with biotinylated plant lectin PHA-L4 (*left*), *Lycopersicon esculentum* agglutinin (*LEA*, *middle*), or AAL (*right*). Goat IgG was used as an isotype control for anti-Mac-2BP capture pAb. Detection levels for HLF-derived Mac-2BP were arbitrarily set at 1. *Error bars* indicate S.D. ($n = 3$). *C*, DC-SIGN recognizes the fucose residues of Le glycans expressed on COLO205-derived Mac-2BP. COLO205 membrane proteins were incubated with or without α1-3,4-fucosidase and then precipitated with rhDC-SIGN-Fc, anti-Le^a or -Le^b mAb, followed by immunoblotting with anti-Mac-2BP pAb. *IP*, immunoprecipitation. *D*, confocal microscopic image of Le^b expression on COLO205-derived Mac-2BP. The cells were costained with anti-Le^b mAb (*green*) and anti-Mac-2BP pAb (*red*). Staining without primary Abs was performed as a negative control. *LP*, ligand precipitation.

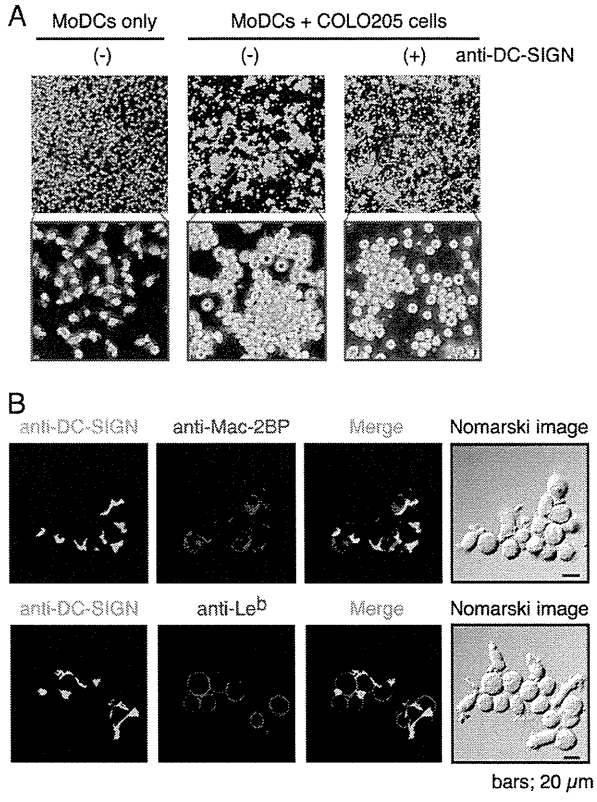

FIGURE 5. **DC-SIGN mediates interaction between MoDCs and COLO205 cells.** *A*, DC-SIGN-dependent cellular adhesions between MoDCs and COLO205 cells. MoDCs only (*left*) or MoDCs plus COLO205 cells in the presence (*right*) or absence (*middle*) of anti-human DC-SIGN pAb were cultured and visualized by phase-contrast microscopy. *B*, confocal microscopic images of MoDC-COLO205 cellular interactions mediated by DC-SIGN and Mac-2BP. MoDCs were cocultured with COLO205 cells. After fixation, cells were stained with anti-human DC-SIGN mAb (*green*) and anti-Mac-BP pAb or anti-Le^b mAb (*red*).

showed that Mac-2BP (*red*) significantly expresses Le^b glycans (*green*) on COLO205 cells (Fig. 4*D*). These results suggest that DC-SIGN is selective in its recognition of specific types of fucosylated *N*-glycans and that these *N*-glycans expressed on DC-SIGN-binding Mac-2BP are important for the interaction.

DC-SIGN Mediates Cellular Adhesion between Immature MoDCs and COLO205 Cells—Next, to determine whether or not immature DCs interact with COLO205 cells through DC-SIGN, we prepared MoDCs from human peripheral blood monocytes and cocultured them with COLO205 cells. As shown in Fig. 5*A*, MoDCs were found to stably adhere to COLO205 cells and to form large agglutinations when they were cocultured (*middle*), compared with a MoDC culture control (*left*). The addition of anti-DC-SIGN pAb partially blocked the MoDC-COLO205 interactions and agglutinations (*right*), indicating that DC-SIGN mediated the interactions and agglutinations. Furthermore, confocal microscopy demonstrated that immature MoDCs expressed a remarkable level of DC-SIGN (*green*) at the points of contact with COLO205 cells

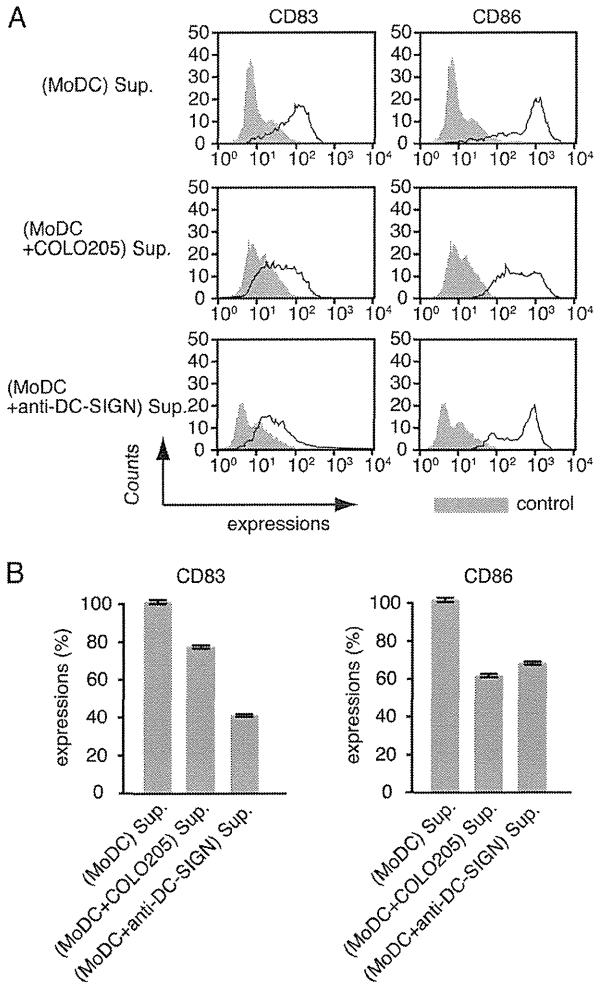

FIGURE 6. **A COLO205-MoDC coculture-derived supernatant suppresses the functional maturation of MoDCs.** *A*, flow cytometry analysis of CD83 and CD86 expressions. Immature MoDCs were incubated with a MoDC-cultured or COLO205-MoDC-cocultured supernatant (*Sup.*) for 3 days in the presence of IL-4, GM-CSF, and LPS (1 ng/ml), and the cultures were replenished with fresh supernatant on the second day. Supernatant of MoDCs, which cultured in the presence of anti-DC-SIGN pAb, was used as a control. The effect on MoDC functional maturation was determined as MoDC surface expression of CD83 and CD86 determined by flow cytometry. *B*, the relative expression levels of CD83 and CD86. The inhibition of MoDC functional maturation was measured as the percentage of mean fluorescent intensity (± S.E.) of incubation with MoDC-cultured supernatant. All experiments were performed in triplicate and were repeated a minimum of three times.

expressing both Mac-2BP (*upper*) and Le^b (*lower, red*) (Fig. 5*B*). These results, also considering the results of Fig. 4, *C* and *D*, suggest that Mac-2BP carrying Le^b glycans is involved in the association between MoDCs and colorectal cancer cells *in situ*.

DC-SIGN-mediated Cellular Adhesion between Immature MoDCs and COLO205 Cells Attenuates MoDC Maturation—We previously demonstrated that the MoDC-SW1116 adhesion mediated by the glycosylation-dependent interactions between DC-SIGN and CEA resulted in dysfunctional MoDCs (9, 10). To determine whether or not this observation is also caused by the DC-SIGN-Mac-2BP interaction, we examined the effect of MoDC-COLO205 coculture condition on MoDC functional maturation. A coculture-derived supernatant was prepared from cocultures of COLO205 carcinoma cells and MoDCs after LPS stimulation. The addition of the MoDC-COLO205 coculture-derived supernatant to a new MoDC culture led to inhibition of maturation marker CD83 and activation marker CD86 expression compared with a MoDC culture-derived control supernatant (Fig. 6, *A* and *B*), suggesting that interaction between MoDCs and COLO205 cells causes suppression of LPS-induced functional maturation of MoDCs. Direct stimulation of MoDC with anti-DC-SIGN pAb also significantly suppressed MoDC maturation, suggesting that the DC-SIGN signaling cascade is sufficiently involved in MoDC maturation pathways. Collectively, our results indicate that the DC-SIGN-dependent interaction with COLO205-derived Mac-2BP as well as that with SW1116-derived CEA induces cellular adhesion between MoDCs and colorectal carcinoma cells, which impairs MoDC functional maturation.

Mac-2BP Is a Major DC-SIGN Ligand in Some Primary Colorectal Carcinoma Tissues—To determine whether or not DC-SIGN recognizes Mac-2BP *in situ*, human normal and malignant colon tissues from the same patients were double stained with rhDC-SIGN and anti-Mac-2BP pAb (Fig. 7*A*). As reported previously (12), Mac-2BP expression in malignant tissues was high in about half of the patients at mucosal epithelia compared with in normal tissues. Moreover, the staining pattern in the rhDC-SIGN markedly overlapped that of the Mac-2BP in the malignant epithelia (Fig. 7*A*), indicating that Mac-2BP, as a novel DC-SIGN ligand, is highly expressed on primary cancer colon epithelia, and implying that DC-SIGN is involved in the association between DCs and colorectal cancer cells *in situ* through recognition of these cancer-related Le glycan ligands.

We and another group (9, 10) have recently reported that DC-SIGN recognizes CEA expressed in colorectal cancer tissues of patients. Therefore, to next examine the differences in expression pattern of and association with rhDC-SIGN between CEA and Mac-2BP, we performed triple staining with rhDC-SIGN, anti-Mac-2BP pAb, and anti-CEA mAb. In contrast to the CEA localization limited on the apical face of cancer epithelia, Mac-2BP expression exhibited a more diffuse pattern on both the apical and basolateral faces of epithelia in malignant colorectal cancer tissues, and little expression of either CEA or Mac-2BP was observed in colorectal normal tissues (Fig. 7*B*). Additionally, as shown in Fig. 7*B*, colorectal cancer patients could be divided into $Mac\text{-}2BP^{high}/CEA^{high}$ (cancer 1), $Mac\text{-}2BP^{low}/CEA^{high}$ (cancer 2 and 3), $Mac\text{-}2BP^{high}/CEA^{low}$ (cancer 4 and 5), and $Mac\text{-}2BP^{low}/CEA^{low}$ (data not shown) groups based on the distinct expression patterns of CEA and Mac-2BP together with the DC-SIGN recognition model. The profiles of Mac-2BP/CEA expression pattern-based groups were shown in Table 1. These results indicate that Mac-2BP may become a novel potential colorectal cancer biomarker for some patients with CEA-low or -negative colorectal cancer.

DISCUSSION

During the neoplastic process in colon tissues, genetic or epigenetic gene alteration often accompanies changes in cell-surface glycans. Glycosylation changes during malignant transformation lead to tumor-specific carbohydrate structures that interact with C-type lectins on dendritic cells. In general, these changes have been associated with a poor prognosis, as they are linked to the aggressiveness and metastatic capacity of tumors.

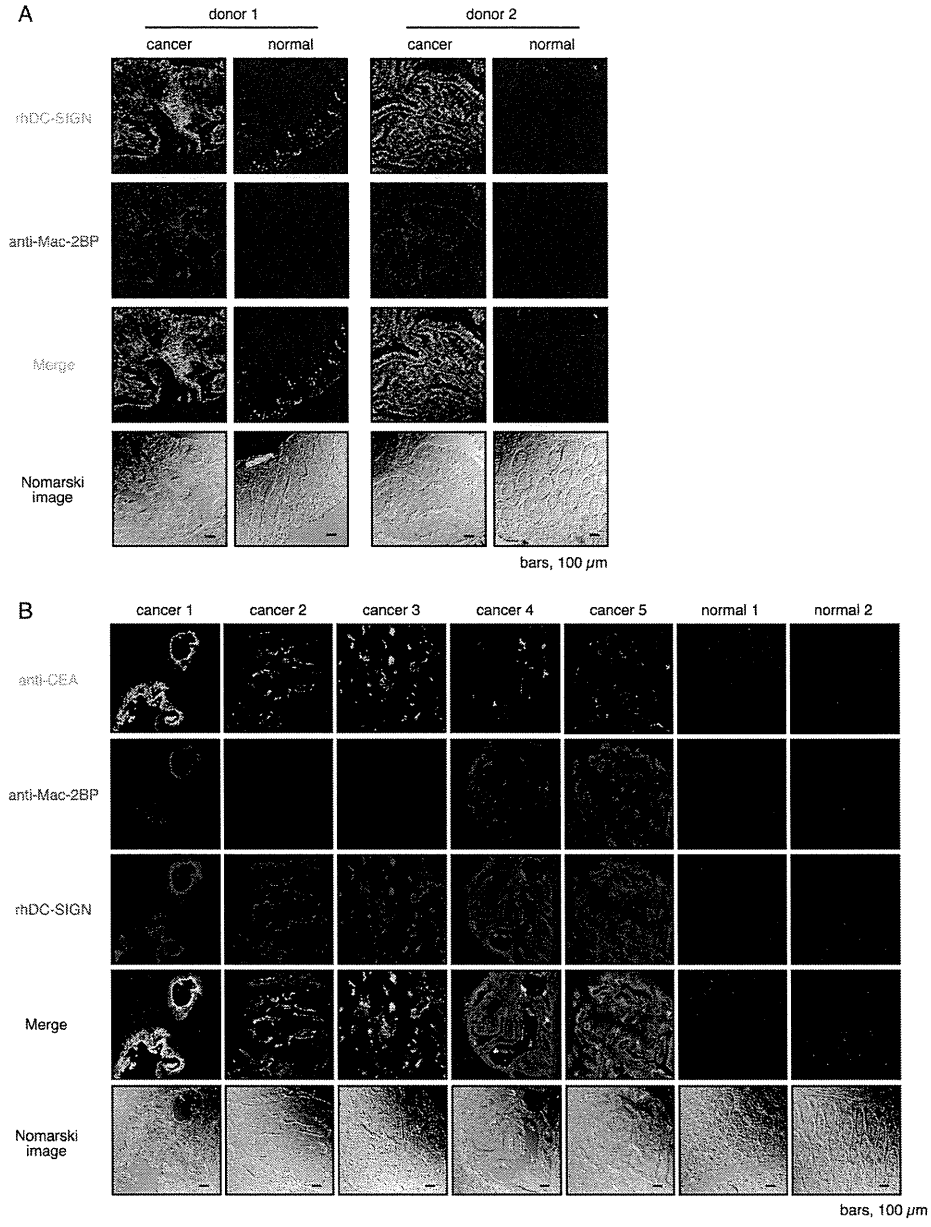

FIGURE 7. **Mac-2BP expressed on colorectal cancer cells is a major target for DC-SIGN *in situ*.** *A*, DC-SIGN recognizes colorectal carcinoma-derived Mac-2BP *in situ*. Primary colorectal cancer and normal colon tissues of donor 1 (SuperBioChips Laboratories) and donor 2 (Shiga University of Medical Science) were stained with rhDC-SIGN (*green*) and anti-Mac-2BP pAb (*red*). *B*, expressions of CEA and Mac-2BP in colorectal tumor tissues (SuperBioChips Laboratories). Triple staining of primary colorectal cancer and normal colon tissues with anti-CEA mAb (*green*), anti-Mac-2BP pAb (*red*), and rhDC-SIGN-allophycocyanin (*blue*). All samples were examined by confocal microscopy.

Good examples of heavily glycosylated tumor antigens are CEA and CEACAM1 (13–19), which can be secreted or expressed by colon cancer cells. Because the function of dendritic cells may be dependent on their binding properties as to self-antigens and pathogens, it is essential to obtain a detailed insight into the carbohydrate-binding properties of DC-SIGN.

Previous research indicated that tumor cells with their surface decorated with β1-6-branched *N*-linked oligosaccharides acquire invasiveness and metastatic potential through a change in the affinity level to the extracellular microenvironment (20, 21). Mac-2BP expressed on colorectal carcinoma cells was initially identified as a L-PHA-recognized major glycoprotein bearing polylactosamine glycans extending from β1-6 branched *N*-linked oligosaccharides (22, 23). In this study, we have firstly identified Mac-2BP on colorectal carcinoma cells as a novel ligand for C-type lectin DC-SIGN and demonstrated the Ca^{2+}-dependent interaction of rhDC-SIGN with Mac-2BP from colorectal carcinoma COLO205 cells. Generally, DC-SIGN exhibits dual specificities for high-mannose as well as Le-type glycans (8, 24, 25). Foreign antigens recognized by DC-SIGN have both types of glycans. Whereas, so far, most endogenous ligands for DC-SIGN have been found to carry only Le-type glycans. Here we showed that specific removal of Le glycans on Mac-2BP by α1-3,4-fucosidase abrogated these interactions, indicating that the fucose moieties of Le glycans are required for the interactions. We also observed that DC-SIGN ligands are highly expressed with Le

TABLE 1

Pathological profile of Mac-2BP/CEA expression patterns in cancer tissues with rhDC-SIGN-staining positive specimens ($n = 16$)

Age	Sex	Organ	Digagnosis	pTNM[a]	Stage[a]	Immunostaining[b] Mac-2BP	CEA
59	M	Ascending colon adenocarcinoma	Moderately differentiated	T3N0M0	II A		
62	M	Sigmoid colon adenocarcinoma	Moderately differentiated	T3N2M1	IV	High	High
41	F	Sigmoid colon adenocarcinoma	Well differentiated	T4N2M1	IV	(16.8%)	
62	M	Ascending colon adenocarcinoma	Moderately differentiated	T3N0M0	II A		
64	M	Sigmoid colon adenocarcinoma	Moderately differentiated	T3N1M0	III B		
75	F	Rectum adenocarcinoma	Well differentiated	T3N1M0	III B	Low	High
68	M	Sigmoid colon adenocarcinoma	Moderately differentiated	T3N1M0	III B	(37.5%)	
65	F	Sigmoid colon adenocarcinoma	Well differentiated	T3N0M0	II A		
56	F	Sigmoid colon adenocarcinoma	Moderately differentiated	T3N2M1	IV		
45	M	Rectum adenocarcinoma	Well differentiated	T3N1M0	III B		
59	M	Sigmoid colon adenocarcinoma	Moderately differentiated	T4N0M0	II B		
62	M	Sigmoid colon adenocarcinoma	Moderately differentiated	T3N0M0	II A	High	Low
57	M	Sigmoid colon adenocarcinoma	Moderately differentiated	T3N0M0	II A	(31.3%)	
46	F	Ascending colon adenocarcinoma	Poorly differentiated	T3N2M0	III C		
60	F	Rectum adenocarcinoma	Moderately differentiated	T4N0M0	II B	Low	Low
47	F	Cecum adenocarcinoma	Moderately differentiated	T3N0M0	II A	(12.5%)	

[a] AJCC Cancer Staging Manual (6th Edition).
[b] Tissue specimens were stained with anti-CEA mAb and anti-Mac-2BP followed by Alexa Fluor-conjugated secondary Abs.

glycans on human colorectal carcinoma cells, suggesting that increased expression of DC-SIGN ligands on colorectal cancer cells in addition to altered glycosylation results in recognition by DC-SIGN and that further fucosylation of polylactosamine glycans and formation of Le epitopes on Mac-2BP during cancer progression may be important for induction of the interaction between DC-SIGN and Mac-2BP. In addition, we also found that the expression levels of Le epitopes were positively correlated with the staining levels with rhDC-SIGN in 30 colorectal carcinoma cell lines, including LoVo, LS513, LS174T, SNU1197, etc. (data not shown).

CEA is one of the most widely used tumor markers for gastrointestinal cancer such as colorectal carcinomas. It has been pointed out that the change in distribution of CEA from apical into basolateral and stromal areas in malignant colorectal cancer tissues could be a cause of its entry into the blood and elevation of the serum CEA levels (14, 16). However, the sensitivity and specificity of CEA are considered to be low, particularly for early stages of the disease such as Dukes A or B stages (26). We showed here that the distribution of Mac-2BP was more basolateral than that of CEA and that expression of Mac-2BP in primary colon adenocarcinoma tissues was increased compared with in proximal normal tissues and obtained various staining patterns for Mac-2BP such as luminal staining and punctate staining on the apical and basolateral faces (Fig. 7*B*). In addition, we observed here that DC-SIGN greatly associated with not only CEA but also Mac-2BP on the apical face of cancer epithelia and that DC-SIGN retained responsiveness to Mac-2BP in more basolateral areas. Because basolateral expression of Mac-2BP has been reported to be more prevalent in early stage Dukes A tumors than in advanced ones (12), DC-SIGN may preferably recognize early stage colorectal carcinoma cells through Mac-2BP. Therefore, similarly to that of CEA, aberrant expression of Mac-2BP and its polar breakdown in cancer tissues may allow its entry into blood vessels. Furthermore, it is also interesting that the type of Mac-2BP secreted by several colorectal carcinoma cells had DC-SIGN-detectable glycan structures, whereas we did not detect any binding of DC-SIGN to serum Mac-2BP from healthy donors (data not shown), suggesting that DC-SIGN can qualitatively distinguish colorectal carcinoma-derived Mac-2BP from serum Mac-2BP in normal and cancer patients.

Recent evidence indicates that dendritic cell-associated DC-SIGN may have functions in both the induction of tolerance to self-antigens and the recognition of pathogens, respectively. A variety of cytokines, including IL-6, IL-10, and macrophage colony-stimulating factor (M-CSF), have been shown to affect the maturation of DCs from $CD34^+$ precursors and from MoDCs *in vitro* (27, 28). Failure of the immune system to provide protection against tumor cells is an important immunological problem. It is now evident that inadequate functioning of the host immune system is one of the main mechanisms by which tumors escape from immune control, as well as an important factor that limits the success of cancer immunotherapy. In recent years, it has become increasingly clear that defects in DCs play a crucial role in non-responsiveness to tumors (29). Here, we showed that DC-SIGN-dependent cellular interactions between immature MoDCs and colorectal carcinoma cells significantly inhibited MoDC functional maturation, suggesting that, similar to CEA, Mac-2BP bearing colorectal tumor-associated Le glycans may provide a tolerogenic microenvironment for colorectal carcinoma cells through interactions with DC-SIGN. These findings also imply that the glycosylation-dependent cellular interactions may result in suppression of DC functions, possibly through immunosuppressive cytokines such as IL-6 and IL-10, and that production of these immunosuppressive factors in DC tumor coculture supernatants may be one of the mechanisms by which tumors evade immunosurveillance.

Recently, the intracellular signaling mechanisms of DC-SIGN were elucidated (30–32). DC-SIGN constitutively associates with a signalosome complex consisting of scaffold protein LSP1 and mediates cross-talk with Toll-like receptor signaling, which results in modulation of Toll-like receptor-induced cytokine responses. Indeed, interaction of foreign pathogens such as *M. tuberculosis* leads to up-regulation of LPS-induced IL-10 and suppresses MoDC maturation (33). Therefore, the MoDC maturation as a consequence of DC-SIGN interacting with Le glycans of cancer cells may also be mediated through a series of LSP1-associated intracellular signaling pathway. MoDCs, following sensitization with CEA-derived peptides *ex vivo*, are now utilized as a tool for the clinical applications of tumor immunotherapies. As the immunogenicities of peptide vaccines vary among patients who exhibit different immune responsiveness, which is defined by means of human leukocyte antigen (HLA) types, etc., appropriate selection of antigens is needed individually to obtain adequate therapeutic benefit. In this context, colorectal carcinoma-derived Mac-2BP, similar to CEA, might become a candidate new cancer vaccine. Canceling of tumor-escaping mechanisms, such as DC-SIGN-mediated MoDC dysfunction, by combination of therapeutic agents that target intracellular signaling molecules (*e.g.* LSP1) may be a critical step for maintaining the effective tumor-immunogenicity in the future.

In conclusion, based on the distinct expression patterns of Mac-2BP and CEA together with the DC-SIGN recognition model presented here, colorectal cancer patients could be divided into $Mac\text{-}2BP^{high}/CEA^{high}$, $Mac\text{-}2BP^{low}/CEA^{high}$,

Mac-2BP^{high}/CEA^{low}, and Mac-2BP^{low}/CEA^{low} groups. The establishment of a model of the DC-SIGN-Mac-2BP/CEA interaction is a valuable step toward elucidation of the physiological function and molecular mechanism and provides a knowledge-based approach for the clinical applications of cancer immunotherapies and novel diagnoses. For this purpose, identification of the DC-SIGN-Mac-2BP/CEA model that breaks immunotolerance to Mac-2BP/CEA and induces cancer immunosurveillance failure both *in vitro* and *in vivo* is therefore a major goal for therapeutic applications in the future.

Acknowledgment—We thank Tomoko Tominaga for secretarial assistance.

REFERENCES

1. Banchereau, J., Briere, F., Caux, C., Davoust, J., Lebecque, S., Liu, Y. J., Pulendran, B., and Palucka, K. (2000) *Annu. Rev. Immunol.* **18,** 767–811
2. Lanzavecchia, A., and Sallusto, F. (2001) *Cell* **106,** 263–266
3. Geijtenbeek, T. B., van Vliet, S. J., Engering, A., 't Hart, B. A., and van Kooyk, Y. (2004) *Annu. Rev. Immunol.* **22,** 33–54
4. van Vliet, S. J., den Dunnen, J., Gringhuis, S. I., Geijtenbeek, T. B., and van Kooyk, Y. (2007) *Curr. Opin. Immunol.* **19,** 435–440
5. van Kooyk, Y., and Rabinovich, G. A. (2008) *Nat. Immunol.* **9,** 593–601
6. Geijtenbeek, T. B., Kwon, D. S., Torensma, R., van Vliet, S. J., van Duijnhoven, G. C., Middel, J., Cornelissen, I. L., Nottet, H. S., KewalRamani, V. N., Littman, D. R., Figdor, C. G., and van Kooyk, Y. (2000) *Cell* **100,** 587–597
7. Geijtenbeek, T. B., Torensma, R., van Vliet, S. J., van Duijnhoven, G. C., Adema, G. J., van Kooyk, Y., and Figdor, C. G. (2000) *Cell* **100,** 575–585
8. van Liempt, E., Bank, C. M., Mehta, P., Garciá-Vallejo, J. J., Kawar, Z. S., Geyer, R., Alvarez, R. A., Cummings, R. D., Kooyk, Y., and van Die, I. (2006) *FEBS Lett.* **580,** 6123–6131
9. van Gisbergen, K. P., Aarnoudse, C. A., Meijer, G. A., Geijtenbeek, T. B., and van Kooyk, Y. (2005) *Cancer Res.* **65,** 5935–5944
10. Nonaka, M., Ma, B. Y., Murai, R., Nakamura, N., Baba, M., Kawasaki, N., Hodohara, K., Asano, S., and Kawasaki, T. (2008) *J. Immunol.* **180,** 3347–3356
11. Grassadonia, A., Tinari, N., Iurisci, I., Piccolo, E., Cumashi, A., Innominato, P., D'Egidio, M., Natoli, C., Piantelli, M., and Iacobelli, S. (2004) *Glycoconj. J.* **19,** 551–556
12. Ulmer, T. A., Keeler, V., Loh, L., Chibbar, R., Torlakovic, E., André, S., Gabius, H. J., and Laferté, S. (2006) *J. Cell Biochem.* **98,** 1351–1366
13. Midiri, G., Amanti, C., Benedetti, M., Campisi, C., Santeusanio, G., Castagna, G., Peronace, L., Di Tondo, U., Di Paola, M., and Pascal, R. R. (1985) *Cancer* **55,** 2624–2629
14. Hamada, Y., Yamamura, M., Hioki, K., Yamamoto, M., Nagura, H., and Watanabe, K. (1985) *Cancer* **55,** 136–141
15. Shi, Z. R., Tsao, D., and Kim, Y. S. (1983) *Cancer Res.* **43,** 4045–4049
16. Ahnen, D. J., Nakane, P. K., and Brown, W. R. (1982) *Cancer* **49,** 2077–2090
17. Nittka, S., Böhm, C., Zentgraf, H., and Neumaier, M. (2008) *Oncogene* **27,** 3721–3728
18. Shively, J. E. (2004) *Oncogene* **23,** 9303–9305
19. Nittka, S., Günther, J., Ebisch, C., Erbersdobler, A., and Neumaier, M. (2004) *Oncogene* **23,** 9306–9313
20. Seelentag, W. K., Li, W. P., Schmitz, S. F., Metzger, U., Aeberhard, P., Heitz, P. U., and Roth, J. (1998) *Cancer Res.* **58,** 5559–5564
21. Dennis, J. W., Laferté, S., Waghorne, C., Breitman, M. L., and Kerbel, R. S. (1987) *Science* **236,** 582–585
22. Laferté, S., and Loh, L. C. (1992) *Biochem. J.* **283,** 193–201
23. Fernandes, B., Sagman, U., Auger, M., Demetrio, M., and Dennis, J. W. (1991) *Cancer Res.* **51,** 718–723
24. Appelmelk, B. J., van Die, I., van Vliet, S. J., Vandenbroucke-Grauls, C. M., Geijtenbeek, T. B., and van Kooyk, Y. (2003) *J. Immunol.* **170,** 1635–1639
25. Guo, Y., Feinberg, H., Conroy, E., Mitchell, D. A., Alvarez, R., Blixt, O., Taylor, M. E., Weis, W. I., and Drickamer, K. (2004) *Nat. Struct. Mol. Biol.* **11,** 591–598
26. Duffy, M. J. (2001) *Clin. Chem.* **47,** 624–630
27. Menetrier-Caux, C., Montmain, G., Dieu, M. C., Bain, C., Favrot, M. C., Caux, C., and Blay, J. Y. (1998) *Blood* **92,** 4778–4791
28. Kiertscher, S. M., Luo, J., Dubinett, S. M., and Roth, M. D. (2000) *J. Immunol.* **164,** 1269–1276
29. Gabrilovich, D. (2004) *Nat. Rev. Immunol.* **4,** 941–952
30. Gringhuis, S. I., den Dunnen, J., Litjens, M., van Het Hof, B., van Kooyk, Y., and Geijtenbeek, T. B. (2007) *Immunity* **26,** 605–616
31. Gringhuis, S. I., van der Vlist, M., van den Berg, L. M., den Dunnen, J., Litjens, M., and Geijtenbeek, T. B. (2010) *Nat. Immunol.* **11,** 419–426
32. Gringhuis, S. I., den Dunnen, J., Litjens, M., van der Vlist, M., and Geijtenbeek, T. B. (2009) *Nat. Immunol.* **10,** 1081–1088
33. Geijtenbeek, T. B., Van Vliet, S. J., Koppel, E. A., Sanchez-Hernandez, M., Vandenbroucke-Grauls, C. M., Appelmelk, B., and Van Kooyk, Y. (2003) *J. Exp. Med.* **197,** 7–17

Glycobiology vol. 22 no. 1 pp. 84–95, 2012
doi:10.1093/glycob/cwr107
Advance Access publication on August 10, 2011

Role of interaction of mannan-binding protein with meprins at the initial step of complement activation in ischemia/reperfusion injury to mouse kidney

Makoto Hirano[2,3,4,8], Bruce Y Ma[3,5,6,9], Nobuko Kawasaki[3], Shogo Oka[7], and Toshisuke Kawasaki[1,3]

[2]Department of Biological Chemistry, Graduate School of Pharmaceutical Sciences, Kyoto University, Kyoto 606-8501, Japan; [3]Research Center for Glycobiotechnology, Ritsumeikan University, Shiga 525-0058, Japan; [4]Institute of Glycoscience, Tokai University, Kanagawa 259-1292, Japan; [5]Department of Computer Science and Systems Engineering, Muroran Institute of Technology, Hokkaido 050-8585, Japan; [6]School of Pharmaceutical Engineering and Life Science, Changzhou University, Jiangsu 213164, People's Republic of China; and [7]School of Health Sciences, Faculty of Medicine, Kyoto University, Kyoto 606-8501, Japan

Received on May 13, 2011; revised on July 20, 2011; accepted on July 29, 2011

Ischemia/reperfusion (I/R) is an important cause of acute renal failure. Recent studies have shown that the complement system mediated by the mannan-binding protein (MBP), which is a C-type serum lectin recognizing mannose, fucose and *N*-acetylglucosamine residues, plays a critical role in the pathogenesis of ischemic acute renal failure. MBP causes complement activation through the MBP lectin pathway and a resulting complement component, C3b, is accumulated on the brush borders of kidney proximal tubules in a renal I/R-operated mouse kidney. However, the initial step of the complement activation has not been studied extensively. We previously identified both meprins α and β, highly glycosylated zinc metalloproteases, localized on kidney proximal tubules as endogenous MBP ligands. In the present study, we demonstrated that serum-type MBP (S-MBP) and C3b were co-localized with meprins on both the cortex and the medulla in the renal I/R-operated mouse kidney. S-MBP was indicated to interact with meprins in vivo in the I/R-operated mouse kidney and was shown to initiate the complement activation through the interaction with meprins in vitro. Taken together, the present study strongly suggested that the binding of S-MBP to meprins triggers the complement activation through the lectin pathway and may cause the acute renal failure due to I/R on kidney transplantation and hemorrhagic shock.

Keywords: cute renal failure / C3b / complement activation / C-type lectin / lectin pathway

Introduction

Ischemia/reperfusion (I/R) is an important cause of acute renal failure. Various clinical conditions such as intravascular volume depletion and hypotension can result in a reduction in renal blood flow, which leads to ischemic acute renal failure (Thadhani et al. 1996). The pathophysiology of renal I/R injury is complicated, but recent studies indicated that activation of complement through the lectin pathway plays a critical role in the pathogenesis of ischemic acute renal failure (de Vries et al. 2004). In the lectin pathway, mannan-binding protein (MBP), also known as mannan-binding lectin (MBL), binds to ligand carbohydrates on the cell surface and activates MBP-associated serine proteases (MASPs). Subsequently, activated MASPs cleave complement components C2 and C4 to yield C3 convertase, which can lead MBP-bound cells to necrosis. However, it is not clear what molecules interact with MBP at the initial stage of the complement activation in renal I/R. Although immunoglobulin M (IgM) triggers the lectin pathway in mesenteric I/R (Zhang et al. 2006), renal I/R does not induce IgM deposition (Park et al. 2002).

MBP recognizes D-mannose, L-fucose and *N*-acetyl-D-glucosamine residues Ca^{2+}-dependently. Human have only one MBP gene, whereas rodents have two MBPs encoded by separate genes, one is serum-type MBP termed S-MBP, MBL-1 or MBL-A and the other is liver-type MBP termed L-MBP, MBL-2 or MBL-C. Both MBPs are mostly synthesized by hepatocytes and secreted into the serum. However, a small amount of S-MBP, but not L-MBP, is synthesized in the mouse (Wagner et al. 2003) and rat (Morio et al. 1997) kidneys. Both mouse S- and L-MBPs can mediate the activation of C4 (Hansen et al. 2000; Liu et al. 2001), although they recognize different bacterial pathogens (Phaneuf et al. 2007).

We previously reported that endogenous MBP ligands are highly expressed on the brush borders of proximal tubules of the normal mouse kidney and the ligands were identified as

[1]To whom correspondence should be addressed: Tel: +81-77-561-3444; Fax: +81-77-561-3444; e-mail: tkawasak@fc.ritsumei.ac.jp
[8]Present address: Institute of Glycoscience, Tokai University, Kanagawa 259-1292, Japan.
[9]Present address: School of Pharmaceutical Engineering and Life Science, Changzhou University, Jiangsu 213164, People's Republic of China.

meprins α and β (Hirano et al. 2005). Meprins are highly glycosylated zinc metalloproteases abundantly expressed in kidney and intestinal epithelial cells, comprising ~5% of the total brush border membrane proteins in the rodent kidneys (Bond and Beynon 1986). Mouse meprin A (EC 3.4.24.18) is a homo-oligomer of α subunits or a hetero-oligomer of α and β subunits (Marchand et al. 1994). Mouse meprin B (EC 3.4.24.63) is a homo-oligomer of β subunits (Gorbea et al. 1993). Meprin α and β subunits form a disulfide-linked dimer and higher-order oligomers through non-covalent interactions (Gorbea et al. 1991). Meprin α has a tendency to form huge complexes with a molecular mass of 1–8 MDa, which comprise 10–100 subunits (Ishmael et al. 2001).

In the present study, we studied the functional role of interaction of MBP with meprins in the I/R-operated mouse kidney, because of the facts that meprins are endogenous ligands for MBP, abundantly expressed in the kidneys and self-aggregate into high-molecular mass complexes that is an important requirement for complement activation to occur. We demonstrated that recombinant mouse S-MBP, but not L-MBP, significantly activated complement by binding to meprins in vitro. Immunohistochemical analysis indicated that S-MBP partially co-localized with meprins in vivo. Additionally, the results of immunoprecipitation (IP) of meprins or S-MBP and in situ proximity ligation assay (PLA; Söderberg et al. 2006) of the renal I/R-operated mouse kidney indicated strongly the functional interaction of S-MBP with meprins in vivo. Protein quantification by western blotting indicated that the amount of S-MBP increased several-fold in the I/R-operated mouse kidney, whereas real-time polymerase chain reaction (PCR) revealed that the amount of S-MBP messenger RNA (mRNA) did not increase in the I/R-operated kidney. These results suggested the possibility that S-MBP increment in the I/R-operated kidney may be due to outflow from the blood circulation rather than the induction of S-MBP mRNA expression in the kidney. Thus, our findings suggested that S-MBP mostly derived from serum interact with meprins and initiates the complement activation through the lectin pathway in renal I/R injury.

Results

Preparation of I/R-operated mice

The experimental renal I/R-operated mouse has been established as a model of acute renal failure. Mice subjected to renal I/R operation exhibited the renal deposition of MBP and complement components and induction of tubular necrosis through the formation of membrane attack complexes (de Vries et al. 2004). We found a high-level expression of endogenous ligands for MBP in the epithelial cells of the kidney proximal tubules and subsequently identified metalloproteases, meprins α and β (meprins) as the predominant MBP ligands (Hirano et al. 2005). Based on this background, we hypothesized that the interaction of MBP with meprins may trigger the activation of complement, resulting in tubular necrosis. In order to test this, we investigated the localization of MBP, meprins and complement component C3b, an activated form of C3, and the protein levels of MBP and meprins, and also the mRNA expression levels of these proteins in the renal I/R-operated mouse kidney. Ischemia was induced by bilateral renal artery clamping and blood urea nitrogen (BUN) was monitored as an index of renal injury. Table I shows BUN level time courses in sham- and I/R-operated mice ($n = 4$). The starting point (0 h) indicates the time when the clamps were removed from the renal arteries. BUN increased gradually during reperfusion and reached at ~3- and 6-fold higher values after 6 and 24 h reperfusion in I/R-operated mice, respectively. We used I/R-operated mice that had reperfused for 6 h in the following experiments.

The localization of meprins, S-MBP and complement C3b in the I/R-operated mouse kidney

Immunohistochemical analysis using a laser confocal microscope indicated marked changes in the distribution of meprin β, S-MBP and C3b in association with I/R operation (Figures 1 and 2). Thus, meprin β was strictly localized in the cortex in the sham-operated mouse kidney (Figure 1A), whereas in the I/R-operated kidney, meprin β was expressed not only in the cortex but also in the medulla significantly (Figure 1G). To the contrary, S-MBP was not detected in the sham-operated kidney (Figure 1B). In the clear contrast to this, in the I/R-operated mouse kidney, S-MBP was massively accumulated in the cortex and, in addition, weak staining was detected in some parts of the medulla (Figure 1H). In higher-magnification views, meprin β in the cortex of the sham-operated mouse kidney was selectively localized on the apical surface of the proximal tubules (Figure 1E). On the other hand, in the I/R-operated mouse kidney, a significant portion of meprin β was detected on the base of the brush border, although there were slight morphological changes in the I/R-operated mouse kidney (Figure 1K). Overlay images indicated that S-MBP was co-localized with meprin β on the base of the brush border of the proximal tubules (Figure 1K) and the medulla (Figure 1L).

Figure 2 indicates that similar changes occurred in the distribution of a complement component, C3b, in association with I/R operation. C3b was hardly detected in the sham-operated mouse kidney (Figure 2B). In the clear contrast, in the I/R-operated mouse kidney, C3b was heavily

Table I. Determination of BUN (mg/dL) before and after renal I/R operation

Time (h)	−0.67	0	1	3	6	12	24
Sham	24 ± 4.3	24 ± 4.1	27 ± 4.4	25 ± 2.8	28 ± 3.0	24 ± 8.0	20 ± 2.8
I/R	25 ± 3.0	32 ± 3.0	38 ± 3.9	56 ± 7.8	73 ± 14.5	124 ± 22.7	160 ± 45.0

Renal function before ischemia (−0.67) and 0, 1, 3, 6, 12 and 24 h after 40 min ischemia. The data are expressed as mean ± SD ($n = 4$).

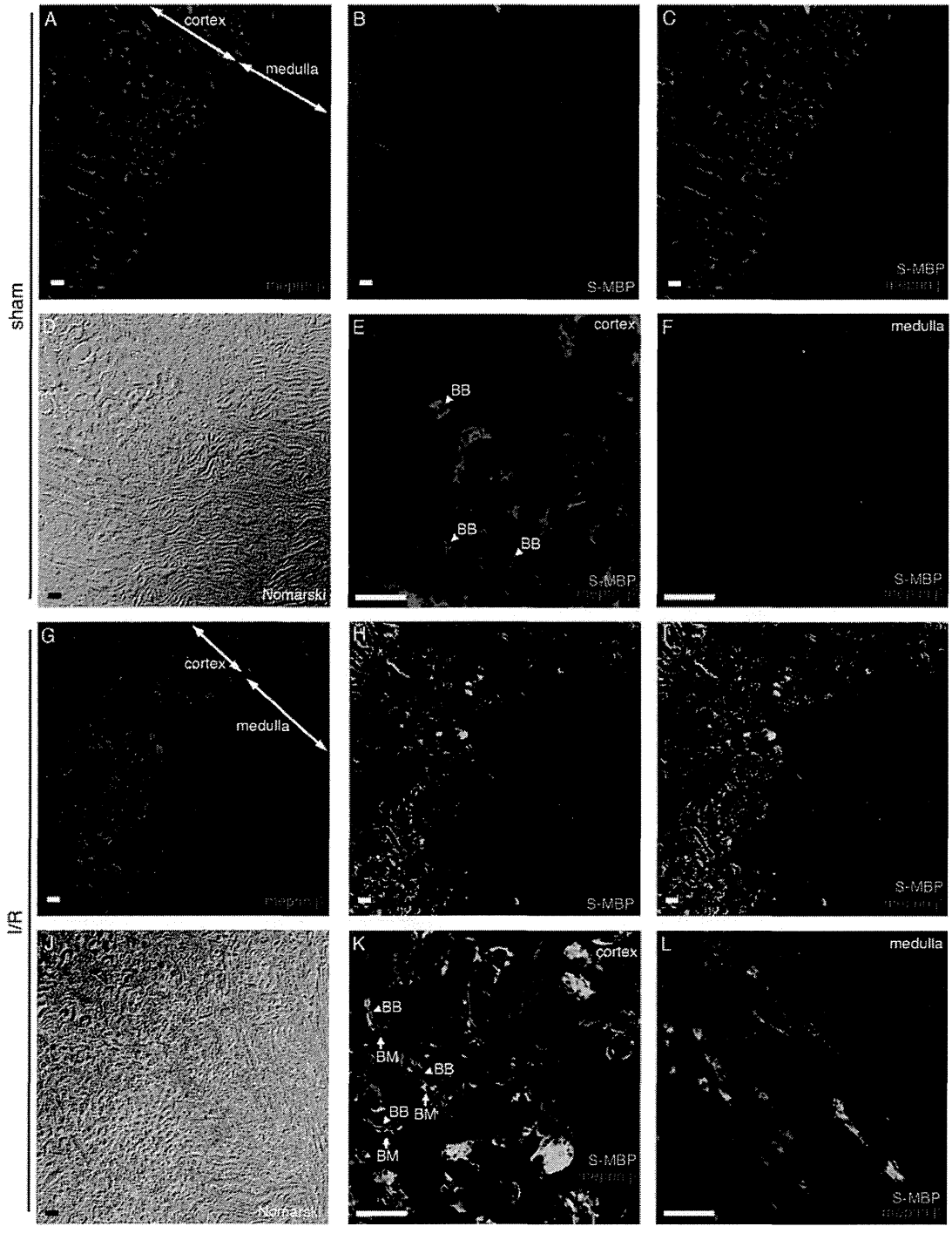

Fig. 1. Localization of S-MBP and meprin β in the renal I/R-operated mouse kidney. Representative kidney paraffin sections (10 μm) were harvested following renal I/R (reperfused for 6 h) and stained with both anti-meprin β and anti-S-MBP antibodies. Cortical and medullary regions are indicated with double arrows in (A) and (G). (**A**) Meprin β (red) was localized strictly in the cortex. (**G**) Meprin β was localized not only in the cortex but also in the medulla. (**B**) S-MBP (green) was not detected. (**H**) S-MBP massively deposited in the cortex and, in addition, S-MBP was weakly detected in the medulla. (**C**) Overlay image of (A) with (B). (**I**) Overlay image of (G) with (H) shows that S-MBP is co-localized with meprin β mostly in the cortex. (**D** and **J**) Nomarski microphotographs of (A)–(C) and (G) and (H), respectively. (**E**, **K**, **F** and **L**) Higher-magnification views of cortical regions of (C) and (I) and medullary regions of (C) and (I), respectively. Arrowheads and arrows indicate the brush border membranes (BB) and the basolateral membranes (BM) of the proximal tubules, respectively. (**E**) Meprin β was strictly localized on the brush border membrane of the proximal tubules, but S-MBP was not detected. (**K**) The brush border membranes of the proximal tubules changed morphologically. S-MBP was partially co-localized with meprin β on the base of the brush border membrane of the proximal tubules. (**F**) Neither S-MBP nor meprin β were detected. (**L**) S-MBP was partially co-localized with meprin β. Bars, 100 μm.

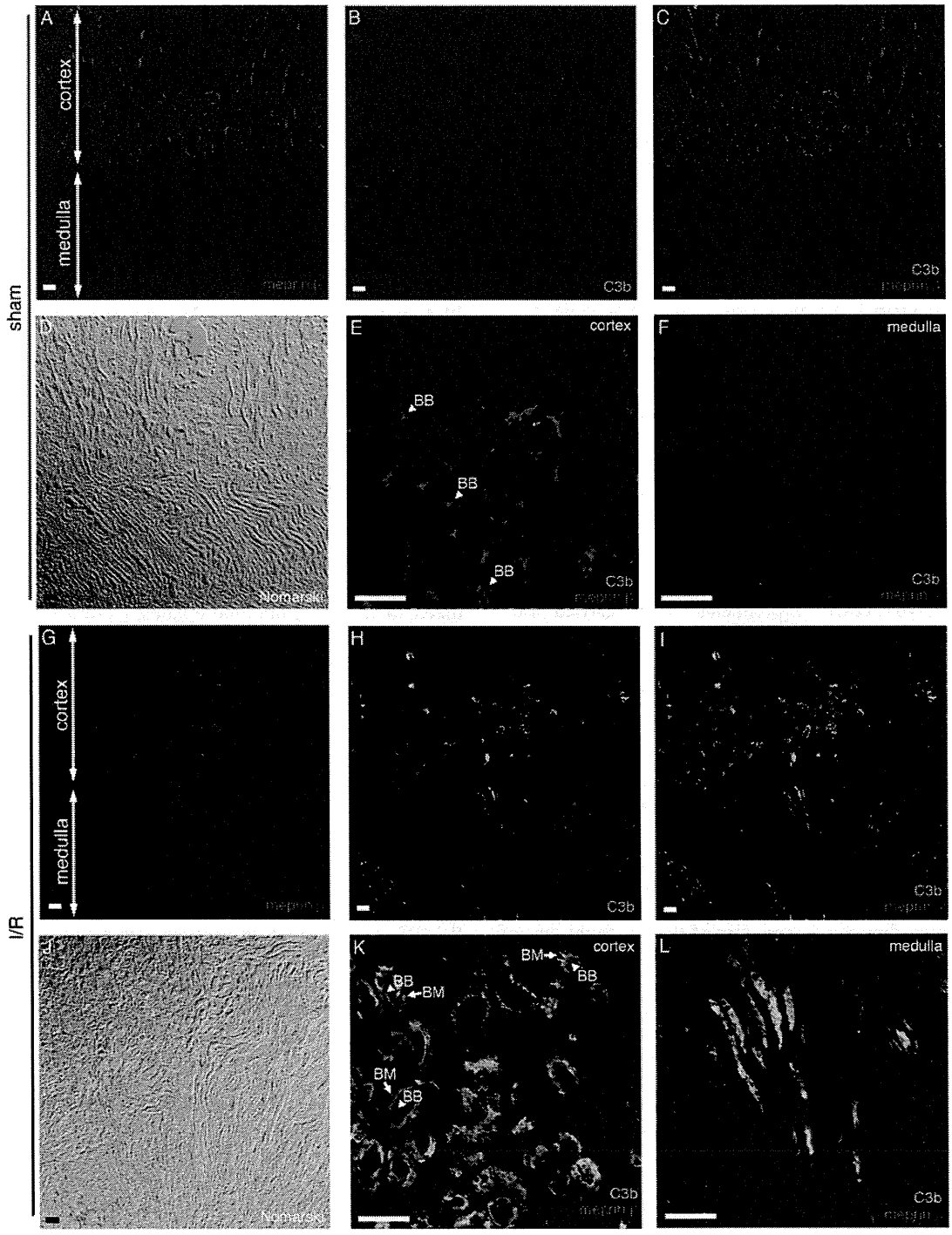

Fig. 2. Localization of C3b and meprin β in the renal I/R-operated mouse kidney. Representative kidney paraffin sections (10 μm) were harvested following renal I/R (reperfused for 6 h) and stained with both anti-meprin β and anti-C3b antibodies. Cortical and medullary regions are indicated with double arrows in (A) and (G). (**A**) Anti-meprin β (red) strictly stained the cortex. (**G**) Anti-meprin β stained not only the cortex but also the medulla. (**B**) C3b (green) was not detected. (**H**) C3b was detected abundantly in the cortex and weakly in the medulla. (**C**) Overlay image of (A) with (B). (**I**) Overlay image of (G) with (H) shows that C3b is co-localized with meprin β mostly in the cortex. (**D** and **J**) Nomarski microphotographs of (A)–(C) and (G) and (H), respectively. (**E**, **K**, **F** and **L**) Higher-magnification views of cortical regions of (C) and (I) and medullary regions of (C) and (I), respectively. Arrowheads and arrows indicate the brush border membranes (BB) and the basolateral membranes (BM) of the proximal tubules, respectively. (**E**) Meprin β was strictly localized on the brush border membrane of the proximal tubules. No signals of C3b were detected. (**K**) C3b was co-localized with meprin β mostly on the base of the brush border membrane of the proximal tubules. (**F**) Neither C3b nor meprin β were detected. (**L**) C3b was partially co-localized with meprin β. Bars, 100 μm.

accumulated in the proximal tubular cells (Figure 2H). C3b was co-localized with meprin β for the most part on the brush border membranes of the proximal tubules (Figure 2K) and in the medulla (Figure 2L).

The immunohistochemical data presented in Figures 1 and 2 indicate clearly that meprin β is an intrinsic component of the normal brush border membranes of the proximal tubules in the cortex, while S-MBP and C3b are not the normal components in this part of the mouse kidney and they appeared only after I/R operation. In addition, the strict localization of meprin β in the cortex was partially abolished and meprin β appeared in the medulla to some extent. Interestingly, S-MBP and C3b, which appeared in the kidney after I/R operation, are co-localized with meprin β on the base of the brush border of the proximal tubules, suggesting a possibility of a functional contact between meprin β and S-MBP. Furthermore, meprin α was co-localized with both S-MBP and C3b in the same manner as meprin β, and L-MBP could not be detected in the kidney (data not shown).

In situ interaction of S-MBP with meprins in the I/R-operated mouse kidney

In order to examine the molecular interaction of S-MBP with meprins in vivo, co-IP experiments were carried out. Small pieces of sham- and I/R-operated mouse kidney cortexes ($n = 3$) were subjected to chemical cross-linking with dithiobis (succinimidylpropionate) (DSP), followed by homogenization and extraction with Nonidet P-40 (NP-40). NP-40 extracts were incubated with antibody specific to S-MBP or meprins, and the immunoprecipitates were analyzed by western blotting after sodium dodecyl sulfate (SDS)–polyacrylamide gel electrophoresis (PAGE). As shown in Figure 3A, multiple S-MBP bands, which probably represent monomer, dimer and trimer of the structural unit of S-MBP, were detected in co-immunoprecipitates with either meprin α (left panel) or meprin β (right panel) as indicated by arrowheads. The estimated molecular masses of trimer, dimer and monomer of the structural unit of S-MBP were 220, 160 and 117 kDa, respectively; in contrast, theoretical molecular masses of trimer, dimer and monomer of the structural unit were ~270, 180 and 90 kDa, respectively. Thus, higher oligomers are estimated to be smaller than their respective theoretical values under non-reducing conditions tested. The reasons for these discrepancies are not clear at the moment but this might be due to incomplete denaturation of higher oligomers because of the presence of intrachain disulfide bonds within the monomeric subunit of S-MBP, interchain disulfide bonds between the subunit components of S-MBP and also newly formed cross-links by DSP treatment. Reversely, as shown in Figure 3B, multiple bands of meprins α and β, probably representing, homo- or heterodimers and trimers of meprins α (left panel) and β (right panel), respectively, were detected in co-immunoprecipitates with S-MBP as indicated by arrowheads. In these two sets of experiments, protein levels of S-MBP and meprins co-immunoprecipitated with meprins and S-MBP, respectively, from the I/R-operated mouse kidney were significantly higher than those from the sham-operated mouse kidney. Furthermore, in the case of the I/R-operated mouse kidney, several larger molecular size bands (indicated by arrows), which probably correspond to DSP cross-linked complexes of S-MBP and meprin β, were observed. It should be noted that the protein bands of meprins and S-MBP, which were immunoprecipitated directly with the same amounts of the respective specific antibodies, were essentially the same either from the I/R-operated mouse kidneys or from the sham-operated mouse kidneys under the conditions examined (data not shown). Taken together, these results indicated that S-MBP and meprins were located close enough to interact with each other in the I/R-operated mouse kidney.

This interaction of S-MBP with meprins in the I/R-operated mouse kidney was further confirmed by in situ PLA of the kidney section. The requirement for dual recombination of pairs of antibodies in combination with very potent signal amplification makes in situ PLA, a powerful tool for identifying numerous interacting proteins and also their subcellular distributions (Söderberg et al. 2006). As shown in the diagram in Figure 3C, when S-MBP and meprins are within 40 nm in proximity, oligonucleotides (plus and minus chains) conjugated with secondary antibodies will hybridize each other to form a circular oligonucleotide. A DNA polymerase will generate a repeated sequence product extended from the circular oligonucleotide as a template. The repeated sequence product will be hybridized to Tex613 fluorophore-labeled oligonucleotide probes. The fluorescent signals indicate the proximity of S-MBP and meprins in situ. As shown in Figure 3D, Tex613 fluorescent signals, which indicate in situ proximity of S-MBP and meprin β, were observed on the base of the brush border of the proximal tubular epithelial cells of the I/R-operated mouse kidney, whereas essentially no signal was detected in the sham-operated mouse kidney. Similarly, essentially no signal was detected in the negative controls that had undergone staining without either primary antibody (neither anti-S-MBP nor anti-meprin β) or without either of the paired primary antibodies (either anti-S-MBP or anti-meprin β) (data not shown). In addition, a signal reflecting the proximity of S-MBP and meprin α was observed in the same manner as for meprin β (data not shown). These results indicate convincingly that S-MBP interacts with meprins in vivo to form macromolecular complexes, which may induce the activation of complement in the I/R-operated mouse kidney.

The activation of complement through the interaction of S-MBP with meprins in vitro

In order to determine whether the interaction of MBP with meprins activates complement, we developed an enzyme-linked immunosorbent assay (ELISA) system involving purified meprins from the normal mouse kidneys and recombinant mouse MBPs. In this assay system, microtiter wells were coated with biotinylated meprins or IgM Fc and filled with or without recombinant mouse S- or L-MBP. Subsequently, human C4 was added to the wells and then the deposited C4b was detected by adding horseradish peroxidase (HRP)-conjugated anti-human C4 monoclonal antibody (mAb). IgM Fc was used as a positive control, since IgM Fc is known to be a good ligand for MBP due to high-mannose-type *N*-glycans attached to the molecule. As shown in Figure 4, meprins demonstrated a remarkable

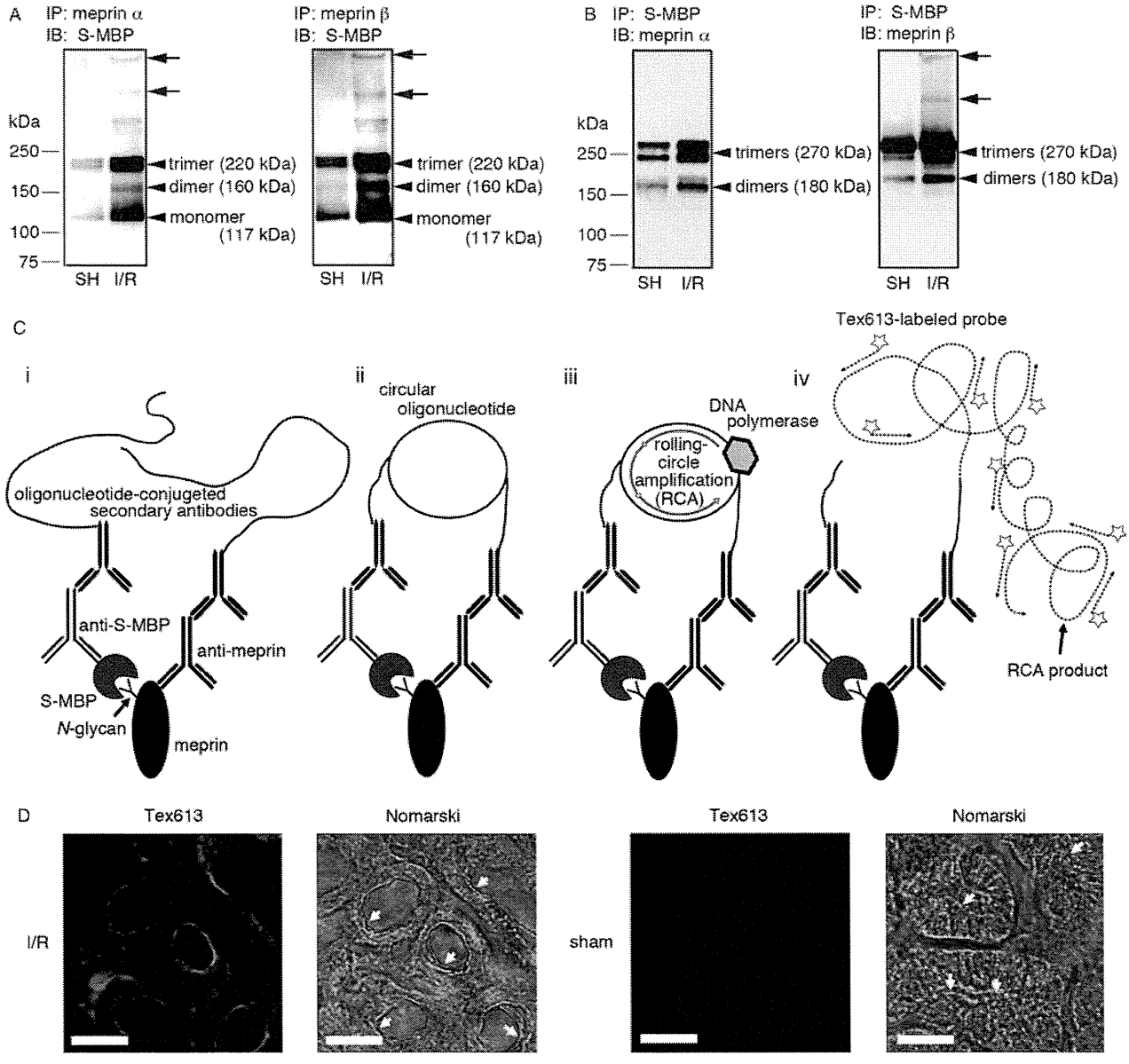

Fig. 3. Interaction of S-MBP with meprins in the I/R-operated mouse kidney. (**A** and **B**) Interaction of S-MBP with meprins after DSP cross-linking. Small pieces of an I/R- and a sham (SH)-operated mouse kidney cortex were cross-linked with 10 mM DSP, and then NP-40 extracts of homogenate were treated with anti-meprin α, anti-meprin β or S-MBP antibody (IP). The complexes were precipitated with Protein G-Sepharose 4B, eluted with SDS–PAGE sample buffer and resolved on a 5–20% Tris–HCl polyacrylamide gradient gel under non-reducing conditions, followed by transfer to nitrocellulose membranes. The immunoblots (IB) were probed with antibodies to S-MBP (A) or meprins (B). The arrows indicate the cross-linked complexes, which consist of S-MBP and meprin α or β. The arrowheads indicate the oligomers of the structural unit of S-MBP and the homo- or hetro-oligomers of meprins on (A) and (B), respectively. (**C**) Diagrams of the principle of in situ PLA. (i) S-MBP and meprin are recognized by specific primary antibodies. Subsequently, the primary antibodies are probed with respective secondary antibodies conjugated with an oligonucleotide (plus or minus chain). (ii) When S-MBP and meprin are within 40 nm in proximity, oligonucleotides will hybridize each other to form a circular oligonucleotide. (iii) A DNA polymerase will generate an RCA product. (iv) The RCA product will be hybridized to a Tex613 fluorophore-labeled probe. The fluorescent signals indicate the proximity of S-MBP and meprin in situ. (**D**) Interaction of S-MBP with meprin β on in situ proximity analysis. Representative kidney paraffin sections (10 μm) were harvested following renal I/R (reperfused for 6 h). The I/R-operated (left two) and the sham-operated (right two) mouse kidneys were used for the in situ proximity assay, as described in *Materials and methods*. The Tex613 signals indicate in situ interaction between S-MBP and meprin β. Arrows indicate the apical surface of the proximal tubules. Bars, 25 μm.

complement activating ability in the presence of S-MBP, which was 4–5-fold higher than that of IgM Fc, this being consistent with the histochemical co-localization of C3b with S-MBP and meprins (Figures 1 and 2). On the other hand, L-MBP did not show essentially any activity under the conditions examined.

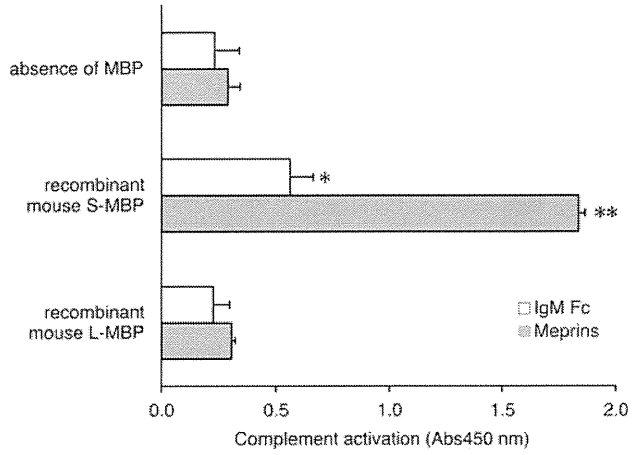

Fig. 4. Activation of complement through the lectin pathway by the interaction of S-MBP and meprins. Each microtiter well was coated with 1.0 μg of biotinylated meprin or IgM Fc and filled with 1.5 μg of recombinant mouse S- or L-MBP. Subsequently, 0.2 μg of human C4 was added to each well and then the deposited C4b was detected by adding HRP-conjugated anti-human C4 mAb, as described in *Materials and methods*. IgM Fc was used as a positive control. Neither S- nor L-MBP was included in the negative controls. The horizontal axis indicates the intensity of C4b deposition in the wells read at 450 nm. All experiments were performed in triplicate and were repeated three times. The data are expressed as means with SD. $*P < 0.05$ and $**P < 0.01$.

Determination of meprins and S-MBP in the I/R-operated mouse kidney

To examine the quantitative changes of meprins and S-MBP in the kidneys in association with I/R operation, we performed western blot analysis of SDS lysates of renal cortex homogenates. Consistent with the result of histochemical studies (see Figure 1), the density of the S-MBP band in the I/R-operated mouse kidney dramatically increased. In contrast, the densities of the meprin α and β bands decreased significantly in the I/R-operated mouse kidney (Figure 5A). Protein was determined as band density, after normalization to the density of β-tubulin (Figure 5B–D). S-MBP increased by almost 5-fold (Figure 5D), whereas both meprins α and β decreased by ~60% (Figure 5B and C). The reason why meprins α and β decreased significantly with I/R operation is not currently clear but it is probably due to partial disorganization of the brush border membrane of the proximal tubular cells, as shown in Figures 1 and 2, where the brush borders seem to be detached from the apical surface on the proximal tubules in the I/R-operated mouse kidney.

The expression of mRNAs of meprins and S-MBP in the I/R-operated mouse kidney

Since S-MBP is expressed in the glomerular mesangial cells of the rat and mouse kidneys (Morio et al. 1997; Wagner et al. 2003), it is possible that I/R operation induces S-MBP expression and increases the quantity of S-MBP protein in the kidney. In order to confirm this, total RNA samples extracted from sham- and I/R-operated mouse kidney cortexes ($n = 6$) were subjected to real-time PCR analysis with target-specific primers. The expression of each mRNA was normalized as to that of glyceraldehyde-3-phosphate dehydrogenase (GAPDH). Figure 5G shows that I/R operation did not increase significantly the expression of S-MBP mRNA. On the other hand, mRNA expression of meprins α and β in the I/R-operated mouse kidneys decreased by 30% (Figure 5E) and 60% (Figure 5F), respectively. These results suggest that the markedly high levels of S-MBP protein after I/R operation might be explained by the influx of S-MBP from the circulation.

Discussion

Recent studies using MBP (S- and L-MBP) double KO mice (Møller-Kristensen et al. 2005) indicated that the complement activation through the MBP lectin pathway plays a critical role in the pathogenesis of ischemic acute renal failure. However, molecular mechanisms of this observation remain unclear. Particularly interesting is the identification of the ligand molecule associated with the initiation of the MBP lectin pathway. We previously identified metalloproteases meprins as endogenous MBP ligands, which are highly expressed in the brush border membranes of kidney proximal tubules (Hirano et al. 2005). However, it was not clear that MBP really interacts with meprins in vivo. Then, we try to clarify this point by focusing on the complement activation through the lectin pathway, which is known to be a major physiological function of MBP.

In the present study, we prepared renal I/R-operated mice as a model of acute renal failure. The immunohistochemical analyses of meprins, MBPs and complement component C3b, which is an activated form of C3, in the I/R-operated mouse kidney revealed marked changes in the distributions of these proteins, and co-localization of meprins with both S-MBP and C3b mainly on the base of the brush border on the proximal tubules. These results suggested the interaction of S-MBP with meprins occurred in the I/R-operated mouse kidney. Co-IP of meprins and S-MBP after chemical cross-linking demonstrated the formation of complexes of meprins and S-MBP, confirming the physical interaction of S-MBP with meprins in vivo, although the formation of cross-linked complexes is not so extensive due probably to a low accessibility of the cross-linking reagent to the site of complex formation on the surface of the cells, since small blocks of kidney tissue were treated with the reagent. Furthermore, in situ PLA (Söderberg et al. 2006) revealed explicitly in situ proximity of S-MBP with meprins on the base of the brush border of the proximal tubules in the I/R-operated mouse kidney. Moreover, the in vitro assay for complement activation demonstrated clearly that the interaction of S-MBP with meprins activated complement more remarkably than that with IgM Fc, which has high-mannose-type *N*-glycans recognized by MBP and is known to be a target of MBP on mesenteric I/R (Zhang et al. 2006). These lines of evidence obtained in this study indicate that S-MBP actually interacts with meprins in situ and that the interaction results in the pathological manifestations by activating complement through the lectin pathway. Bylander et al. (2008) reported that meprin β deficiency prevents renal I/R injury. In meprin β KO mice, secreting-type meprin α is not retained on the brush border membranes of the kidney